2. Convective-Stratiform Separation

This section summarizes the work performed in FY02 toward the development of a real-time automatic convective-stratiform classifier called the Convective-Stratiform Separation Algorithm (CSSA). This classifier supports the new Range Correction Algorithm (RCA), an algorithm to correct real-time operational WSR-88D rainfall estimates for nonuniform vertical profiles of reflectivity (VPR) (Seo et al. 2000) which is currently being software-engineered for implementation in the WSR-88D Open Radar Product Generator (ORPG).

2.1 Introduction

In the RCA algorithm of Seo et al. (2000), estimation of mean VPR and application of the resulting correction factors are carried out over the entire 3-dimensional scanning domain of the radar, rather than locally, due to computational and sampling reasons (Seo et al. 2000, Vignal et al. 2000). Studies indicate that, while radar umbrella-wide estimation and correction of VPR effects works well for widespread pure stratiform events (Seo et al. 2000), such a practice can be counterproductive in situations of embedded convection (Vignal et al. 2000) as explained below. Because convective cores generally occupy only a small fraction of the entire precipitation area, mean VPR is reflective more of the reflectivity morphology of stratiform precipitation than that of convective precipitation. As such, application of the adjustment factors derived from mean VPR to convective cores results, in general, in overestimation of rainfall (assuming, of course, that the Z-R parameters are reasonable). For this reason, automatic recognition and separation of convective cores from stratiform precipitation is considered a requisite for routine implementation of VPR correction. The net effect sought from this two-step approach of 1) convective-stratiform separation and 2) mean VPR estimation and correction (both limited to stratiform area only) is essentially local VPR correction (Vignal et al. 2000).

In FY01, exploratory analysis was carried out to identify attributes that are skillful in separating convective cores from the stratiform background (or vice versa) (see the summary in Fulton et al. 2001). The purpose of this work is to develop an automatic algorithm that quantifies, in probabilistic terms, the likelihood of an azimuth-range (az-ran) bin belonging to the convective/stratiform area based on these attributes.

2.2 Methodology

As summarized in Fulton et al. (2001), a number of candidate techniques are available for probabilistic classification. As suggested in Fulton et al. (2001), we use in this work the indicator approach (Deutch and Journel 1992, Seo 1996) as an approximation to the multivariate probability, Prob[Bin $\in$ convective (or stratiform) | attribute$_1$ < (or $\geq$) threshold$_{1,i1}$, attribute$_2$ < (or $\geq$) threshold$_{2,i2}$,..., attribute$_n$ < (or $\geq$) threshold$_{n,in}$; i_1=1,...,m_1; i_2=1,...,m_2;...;i_n=1,...,m_n], where n is the total number of attributes employed, and m_1 through m_n denote the number of thresholds used for attributes 1 through n, respectively.

As summarized in Fulton et al. (2001), a number of attributes were examined in FY01 that may possess significant skill in discriminating convective cores from stratiform background (or vice versa). It was found that the following three are particularly skillful; maximum reflectivity in the vertical (denoted as r_x), vertically-averaged local spatial correlation of reflectivity (denoted as ρ_r), and local spatial correlation of the top-height of apparent convective core (denoted as ρ_h). The apparent convective core is defined as any az-ran bin in the vertical exceeding 35 dBZ (an adaptable parameter). The correlation-based attributes, ρ_r and ρ_h, are defined as the minima of the correlation coefficients along the radial and the azimuthal directions; i.e., $\rho_r = \min\{ \rho_{r,radial}, \rho_{r,azimuthal} \}$ and $\rho_h = \min\{ \rho_{h,radial}, \rho_{h,azimuthal} \}$. As will be seen, additional attributes were also examined in this work for possible inclusion in the conditioning set, such as the reflectivity gradient in the vertical above the height of maximum reflectivity and the vertically-integrated liquid water content (VIL).

Given the three attributes, r_x, ρ_r, and ρ_h, the problem is then to estimate the conditional probability that any given az-ran bin may belong to the convective or stratiform area of precipitation. In the indicator approach, the conditioning variables are not the absolute magnitude of the attributes themselves, but only their binary encoding, based on whether the attributes are greater or less than some preset thresholds. Here, we formulate the estimator as Prob[Bin $\in$ stratiform | $r_x < r_{xci}$, $\rho_r \geq \rho_{rcj}$, $\rho_h \geq \rho_{hck}$; i=1,...,n_1, j=1,...,n_2, k=1,...,n_3], where n_1, n_2 and n_3 denote the number of thresholds used for r_x, ρ_r and ρ_h, respectively. We then approximate the above conditional probability with the following conditional expectation involving indicator variables (i.e., the binary rendition of the attributes via thresholding):

$$\text{Prob}[\text{ Bin} \in \text{stratiform} \mid r_x < r_{xci},\ \rho_r \geq \rho_{rcj},\ \rho_h \geq \rho_{hck};\ i=1,...,n_1,\ j=1,...,n_2,\ k=1,...,n_3\ ]$$

$$\approx E[I_s \mid I_{rxi} = i_{rxi},\ I_{\rho rj} = i_{\rho rj},\ I_{\rho hk} = i_{\rho hk};\ i=1,...,n_1,\ j=1,...,n_2,\ k=1,...,n_3\ ] \quad (1)$$

In the above and throughout this section, random variables are denoted by upper case letters and the outcome of the random variables by the corresponding lowercase letters. In Eq.(1), r_{xci}, ρ_{rcj} and ρ_{hck} are the i-th, j-th and k-th thresholds for r_x, ρ_r and ρ_h, respectively, and the indicator variables, I_s, I_{rxi}, $I_{\rho rj}$ and $I_{\rho hk}$ are defined as:

$$i_s = \begin{cases} 0 & \text{if the bin is in the convective core} \\ 1 & \text{otherwise} \end{cases} \quad (2)$$

$$i_{rxi} = \begin{cases} 1 & \text{if } r_{xi} < r_{xci} \\ 0 & \text{otherwise} \end{cases} \quad (3)$$

$$i_{\rho rj} = \begin{cases} 0 & \text{if } \rho_{rj} < \rho_{rcj} \\ 1 & \text{if otherwise} \end{cases} \quad (4)$$

$$i_{\rho hk} = \begin{cases} 0 & \text{if } \rho_{hk} < \rho_{hck} \\ 1 & \text{otherwise} \end{cases} \quad (5)$$

The conditional expectation of I_s is estimated by the following linear estimator:

$$E[I_s \mid I_{rxi} = i_{rxi},\ I_{\rho rj} = i_{\rho rj},\ I_{\rho hk} = i_{\rho hk};\ i=1,...,n_1,\ j=1,...,n_2,\ k=1,...,n_3\ ]$$
$$= \sum_{i=1}^{n_i} \lambda_{rxi}\, i_{rxi} + \sum_{j=1}^{n_j} \lambda_{\rho rj}\, i_{\rho rj} + \sum_{k=1}^{n_k} \lambda_{\rho hk}\, i_{\rho hk} \qquad (6)$$

where λ_{rxi}, $\lambda_{\rho rj}$ and $\lambda_{\rho hk}$ denote the weights associated with the indicator variables.

Note in the above development that we could have just as easily formulated the estimator in terms of the bin belonging to the convective core, i.e., Prob[bin $\in$ convective $\mid r_x \geq r_{xci}$, $\rho_r < \rho_{rcj}$, $\rho_h < \rho_{hck}$; i=1,...,n_1, j=1,...,n_2, k=1,...,n_3]. Examination of the conditional probability structure, however, indicates that the stratiform formulation in Eq.(1) is preferable and, in fact, produces better results (not shown). The weights, λ_{rxi}, $\lambda_{\rho rj}$ and $\lambda_{\rho hk}$, are obtained by solving the following indicator version of ordinary kriging (see, e.g., Deutsch and Journel 1992):

$$\text{Minimize } J = E[(I_s - I_s^*)^2 \mid I_{rx} = i_{rxi},\ I_{\rho r} = i_{\rho rj},\ I_{\rho h} = i_{\rho hk};\ i=1,...,n_1,\ j=1,...,n_2,\ k=1,...,n_3\ ] \qquad (7)$$

subject to

$$\sum_{i=1}^{n_1} \lambda_{rxi} + \sum_{j=1}^{n_2} \lambda_{\rho rj} + \sum_{k=1}^{n_3} \lambda_{\rho hk} = 1 \qquad (8)$$

where I_s^* in Eq.(7) is given by Eq.(6). The above constrained minimization is identical to ordinary kriging, for which the weights are obtained by solving the following linear system:

$$\begin{bmatrix} \mathbf{Cov(I_{rx},I_{rx})} & \mathbf{Cov(I_{rx},I_{\rho r})} & \mathbf{Cov(I_{rx},I_{\rho h})} & \mathbf{U_1}^T \\ \mathbf{Cov(I_{\rho r},I_{rx})} & \mathbf{Cov(I_{\rho r},I_{\rho r})} & \mathbf{Cov(I_{\rho r},I_{\rho h})} & \mathbf{U_2}^T \\ \mathbf{Cov(I_{\rho h},I_{rx})} & \mathbf{Cov(I_{\rho h},I_{\rho r})} & \mathbf{Cov(I_{\rho h},I_{\rho h})} & \mathbf{U_3}^T \\ \mathbf{U_1} & \mathbf{U_2} & \mathbf{U_3} & 0 \end{bmatrix} \begin{bmatrix} \boldsymbol{\lambda_{rx}} \\ \boldsymbol{\lambda_{\rho r}} \\ \boldsymbol{\lambda_{\rho h}} \\ \mu \end{bmatrix} = \begin{bmatrix} \mathbf{Cov(I_s,I_{rx})} \\ \mathbf{Cov(I_s,I_{\rho r})} \\ \mathbf{Cov(I_s,I_{\rho h})} \\ 1 \end{bmatrix} \qquad (9)$$

In the above, μ is the Lagrange multiplier, $\mathbf{U_1}$ is the (1xn_1) unit vector; $\mathbf{U}$=(1,1,..,1), $\mathbf{Cov(I_s,I_{rx})}$ is the (n_1x1) indicator covariance vector; $\mathbf{Cov(I_s,I_{rx})} = [\mathrm{Cov}(I_s,I_{rx1}),...,\mathrm{Cov}(I_s,I_{rxn1})]^T$, and $\mathbf{Cov(I_{rx},I_{\rho r})}$ the (n_1xn_2) indicator covariance matrix;

$$\mathbf{Cov(I_{rx},I_{\rho r})} = \begin{bmatrix} \mathrm{Cov}(I_{rx1},I_{\rho r1})...\mathrm{Cov}(I_{rx1},I_{\rho rn2}) \\ \mathrm{Cov}(I_{rx2},I_{\rho r1})...\mathrm{Cov}(I_{rx2},I_{\rho rn2}) \\ . \\ \mathrm{Cov}(I_{rxn1},I_{\rho r1})...\mathrm{Cov}(I_{rxn1},I_{\rho rn2}) \end{bmatrix} \qquad (10)$$

In a nutshell, the indicator approach described above approximates multivariate probability

with a set of bivariate probabilities. For example, note that $Cov(I_s,I_{rx1})$ in $\mathbf{Cov(I_s,I_{rx})}$ may be rewritten as:

$$Cov(I_s,I_{rx1})$$

$$= E[I_s\, I_{rx1}] - E[I_s]\, E[I_{rx1}] \qquad (11a)$$

$$= Prob[\ Bin \in stratiform,\ r_x < r_{xc1}\ ] - Prob[\ Bin \in stratiform\ ]\ Prob[\ r_x < r_{xc1}\ ] \qquad (11b)$$

$$= \{\ Prob[\ Bin \in stratiform \mid r_x < r_{xc1}\ ] - Prob[\ Bin \in stratiform\ ]\ \}\ Prob[\ r_x < r_{xc1}\ ] \qquad (11c)$$

Hence, if the maximum reflectivity in the vertical is indeed a skillful attribute in discriminating convective cores from the stratiform area (or vice versa), the conditional probability, $Prob[\ Bin \in stratiform \mid r_x < r_{xc1}\ ]$, should be greater than the unconditional probability, $Prob[\ Bin \in stratiform\ ]$ (thus resulting in a positive indicator covariance). In this way, the indicator approach also facilitates systematic assessment of the skill level of candidate attributes in a simplified (bivariate, as opposed to multi-variate) manner.

2.3 Estimation of Indicator Statistics

Preferably, the covariance terms in Eq.(9) should be estimated climatologically, stratified according to season and, if necessary, synoptic conditions in a site-specific manner. From an algorithmic point of view, such climatological estimation is not an issue in that climatological indicator statistics can easily be updated recursively on line via, e.g., exponential smoothing (Schweppe 1973). From an operational point of view, however, such estimation does pose a problem in that ground-truthing (i.e. delineating the 'true' convective core) would require human (i.e., the forecaster) interface. For that reason, the working assumption in this work is that rigorous or site-specific estimates of climatological indicator statistics will not be available in the operational implementation of the algorithm, and that the algorithm must work reasonably well even if the indicator covariance estimates may be significantly off from the 'optimal.' Here, we estimate the covariance terms in Eq.(9) only from a single event, a classic southern plains squall line at KINX (Tulsa, OK) (see Table 1). This choice is motivated by the fact that the storm has a very well-defined convective front followed by a well-defined trailing stratiform region (and hence leaves little doubt as to where the 'true' convective core is), and that an operational separation technique has to perform reasonably well even if the covariance structure is subject to large uncertainties (and hence offers a more stringent test for the separation technique).

Figs. 1, 3, 5, 8, 14, 16, and 21 show the maximum reflectivity (r_x) fields for volume scans 245, 255, 265, 275, 285, 295 and 305, respectively, during the event at KINX. The sequence captures the passage of a well-developed squall line with well-defined convective leading edge and stratiform trailing region within the radar umbrella. In each figure, the straight line denotes the

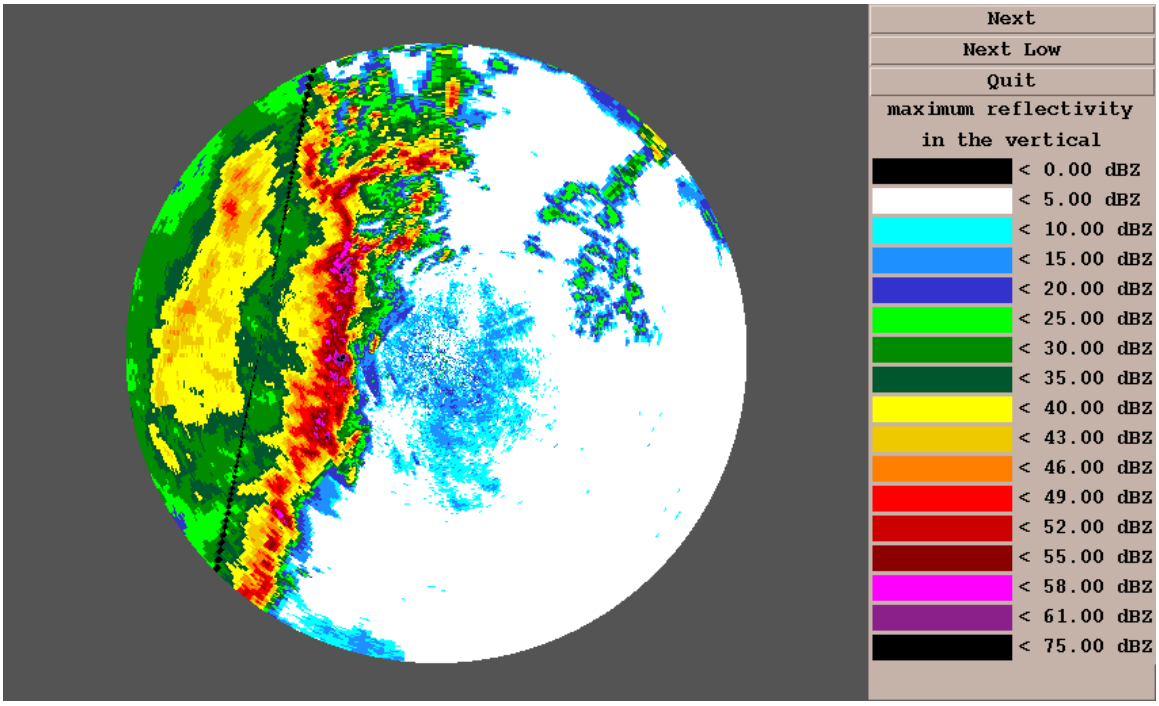

Fig 1 Maximum reflectivity in the vertical, r_x (KINX_N04206 VS_245)

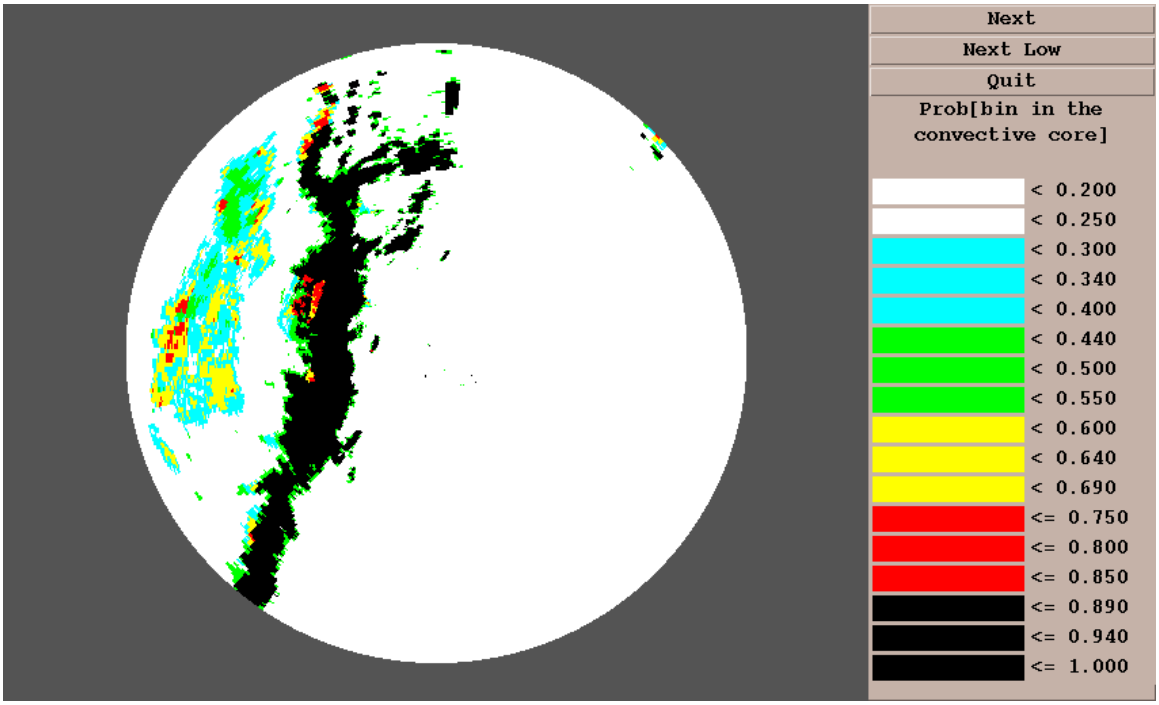

Fig 2 Prob [Bin $\in$ convective | •] (KINX_N04206 VS_245)

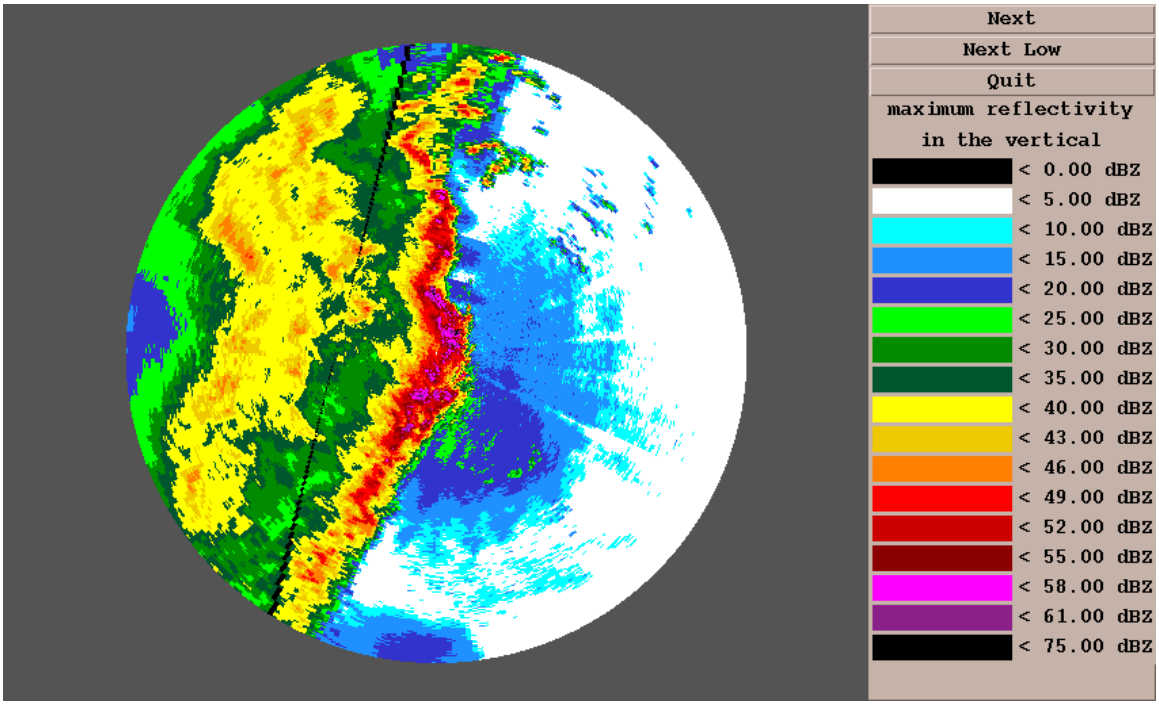

Fig 3 Maximum reflectivity in the vertical, r_x (KINX_N04206 VS_255)

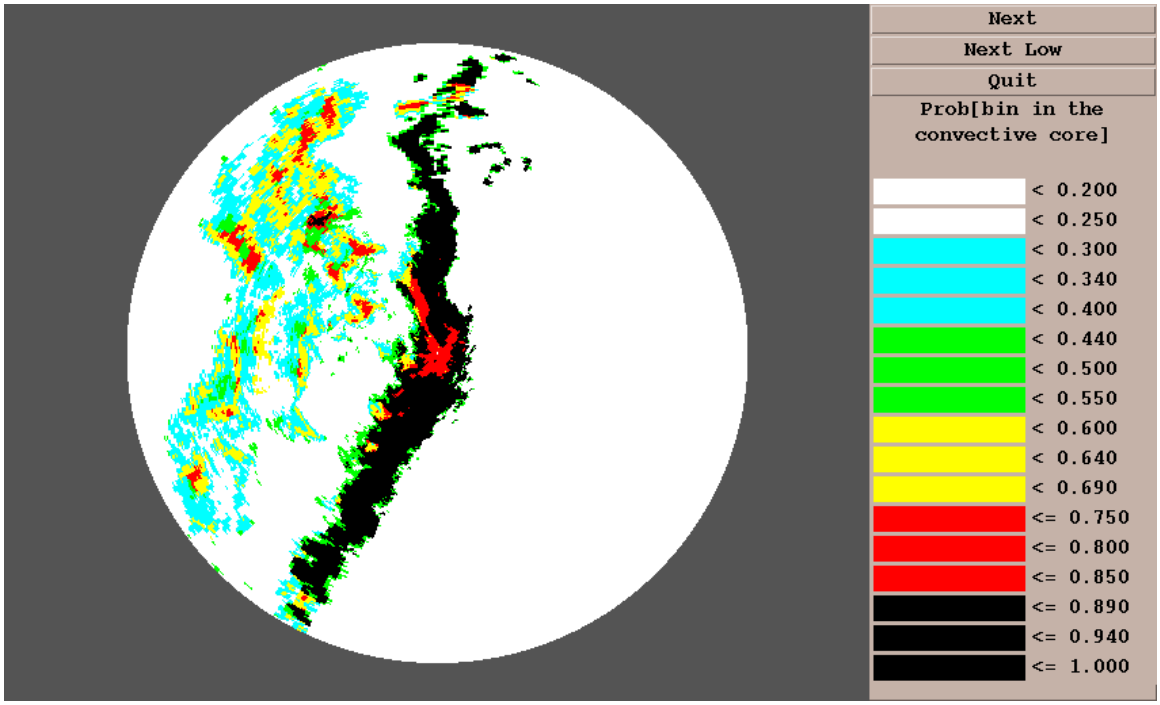

Fig 4 Prob [Bin $\in$ convective | •] (KINX_N04206 VS_255)

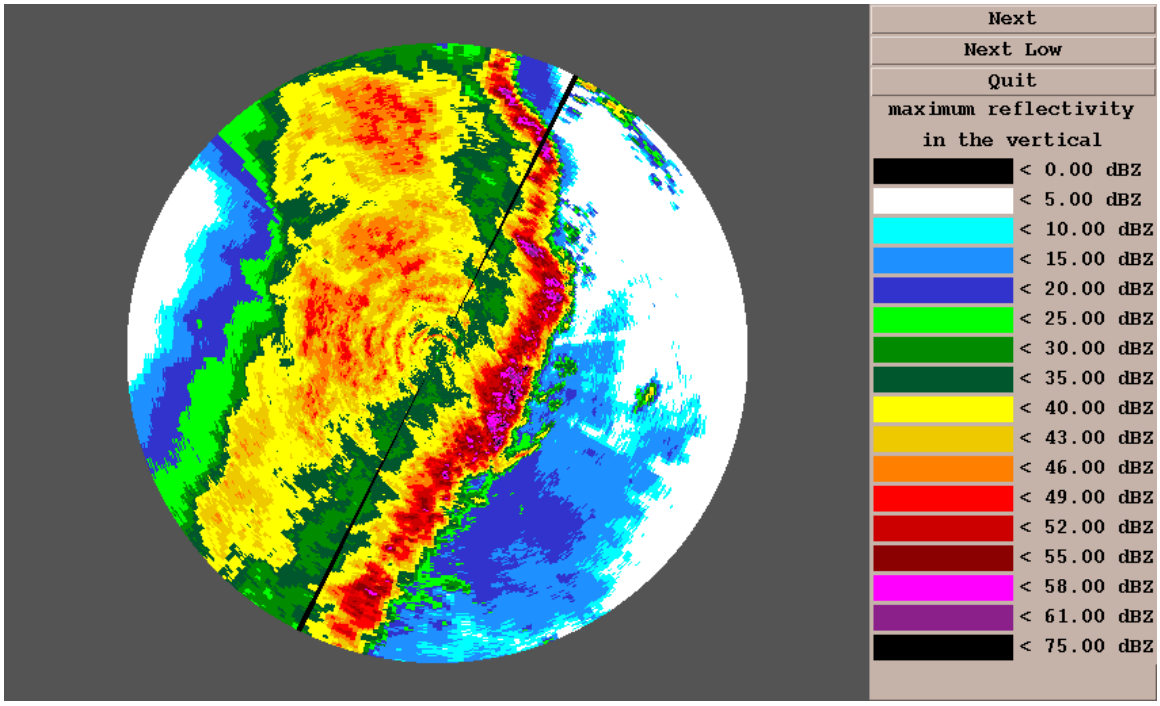

Fig 5 Maximum reflectivity in the vertical, r_x (KINX_N04206 VS_265)

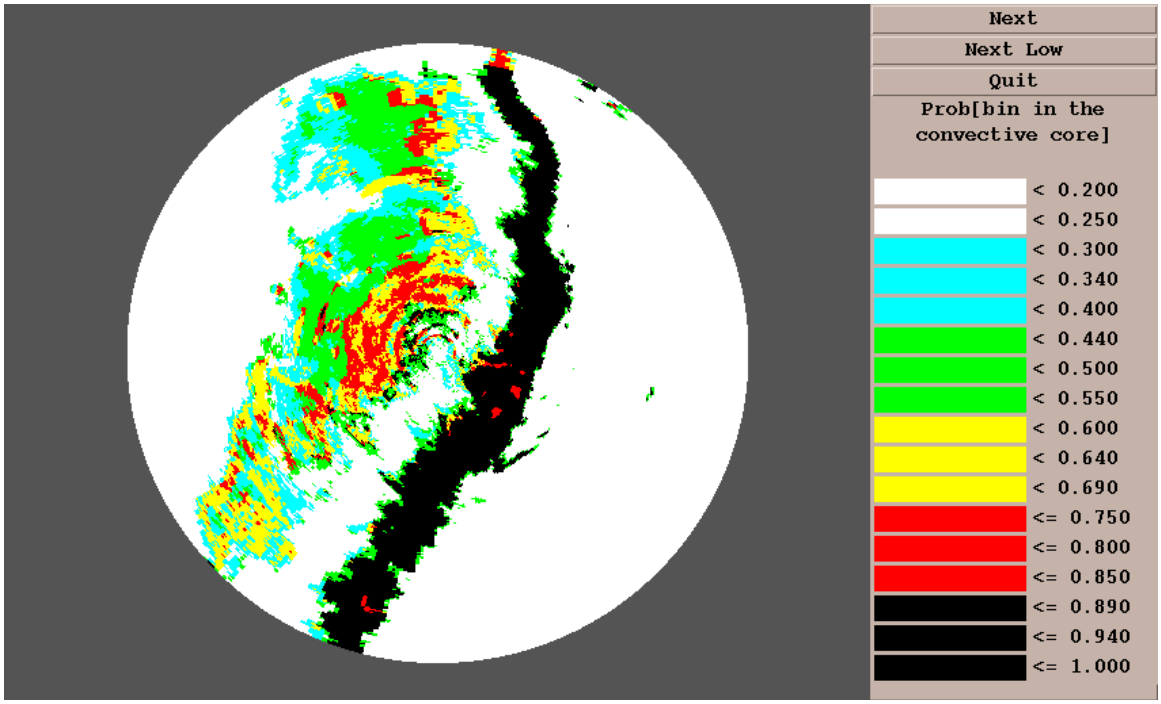

Fig 6 Prob [Bin $\in$ convective | •] (KINX_N04206 VS_265)

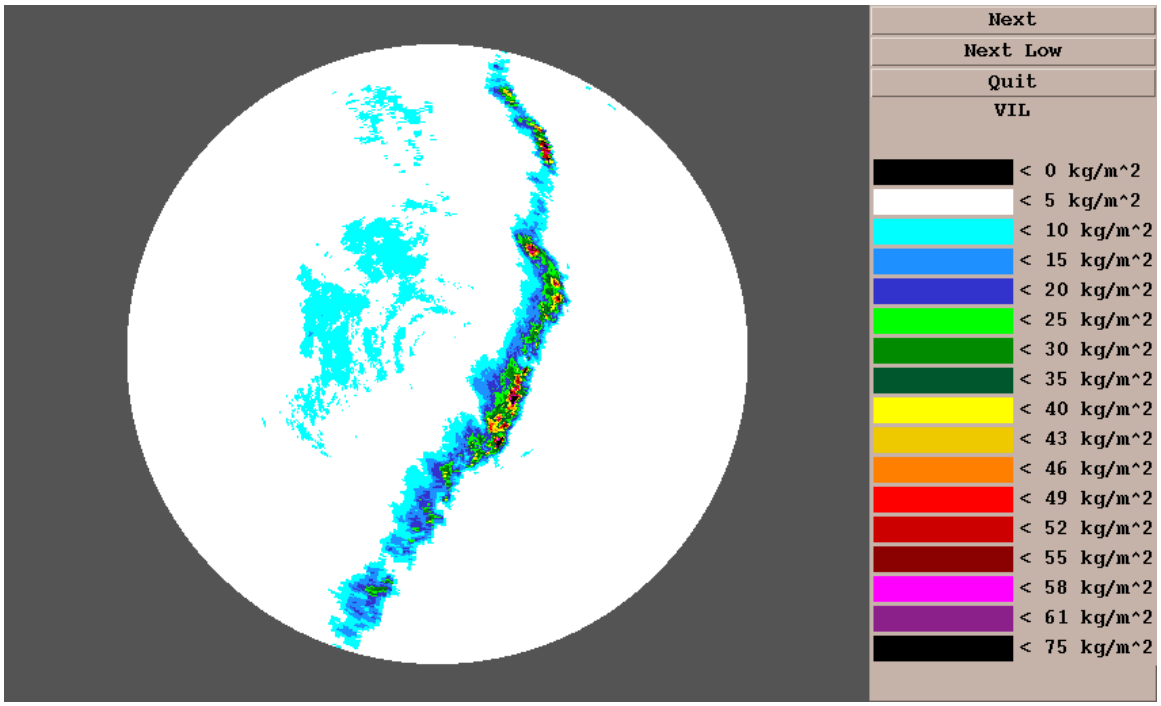

Fig 7 Vertically-integrated liquid water content (VIL) (KINX_N04206 VS_265)

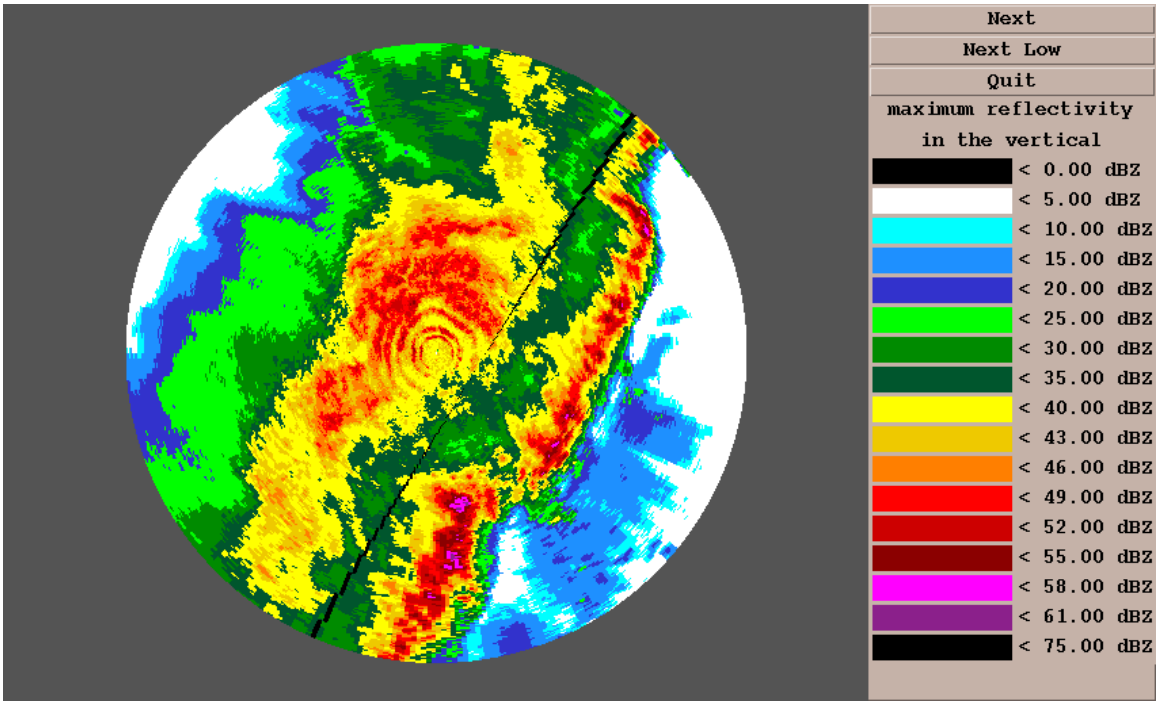

Fig 8 Maximum reflectivity in the vertical, r_x (KINX_N04206 VS_275)

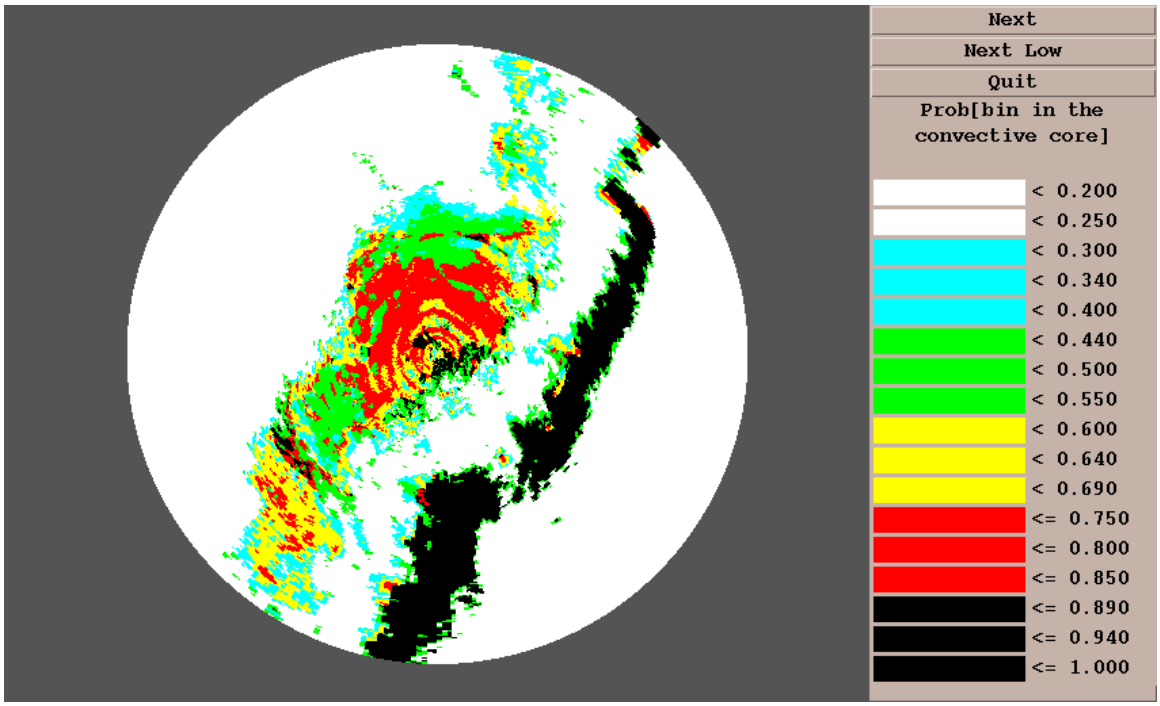

Fig 9 Prob [Bin $\in$ convective | •] (KINX_N04206 VS_275)

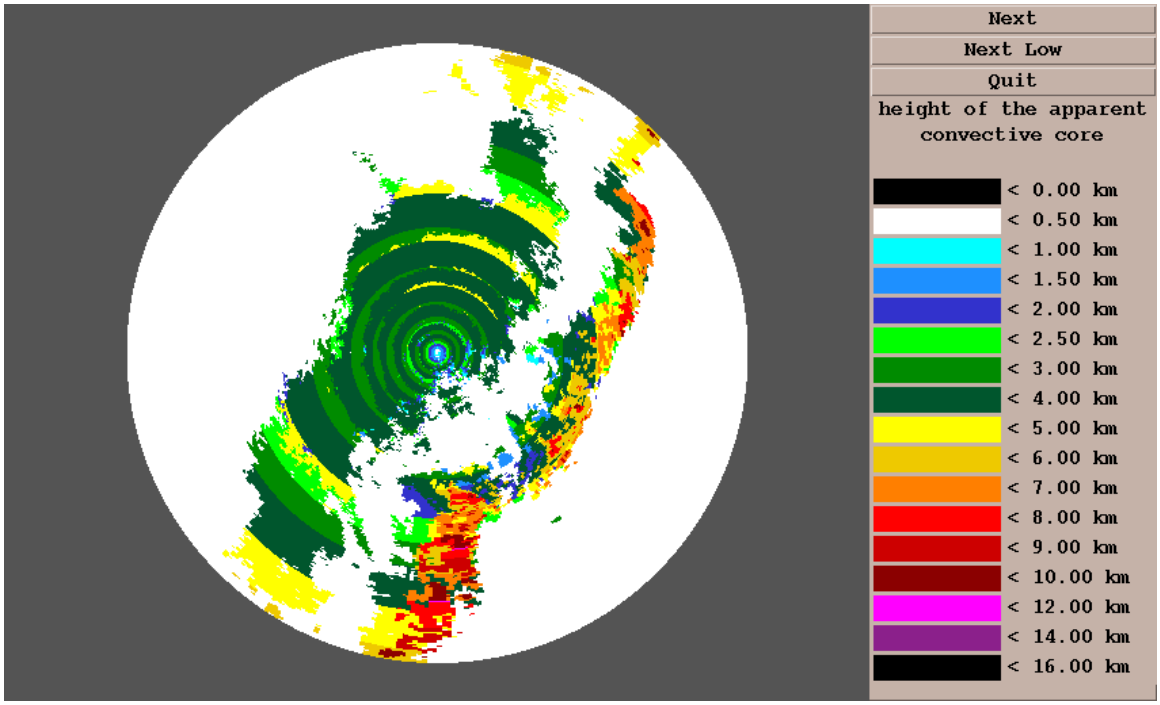

Fig 10 Top height of apparent convective core (KINX_N04206 VS_275)

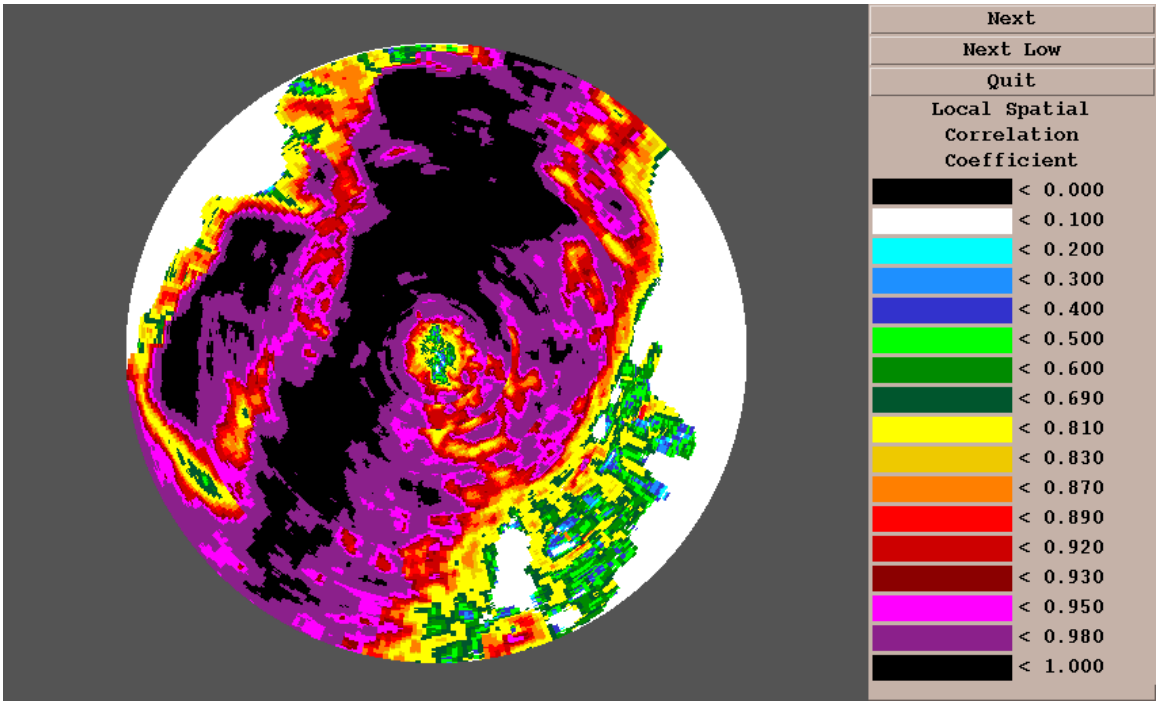

Fig 11 Vertically-averaged spatial correlation of reflectivity, ρ_r (KINX_N04206 VS_275)

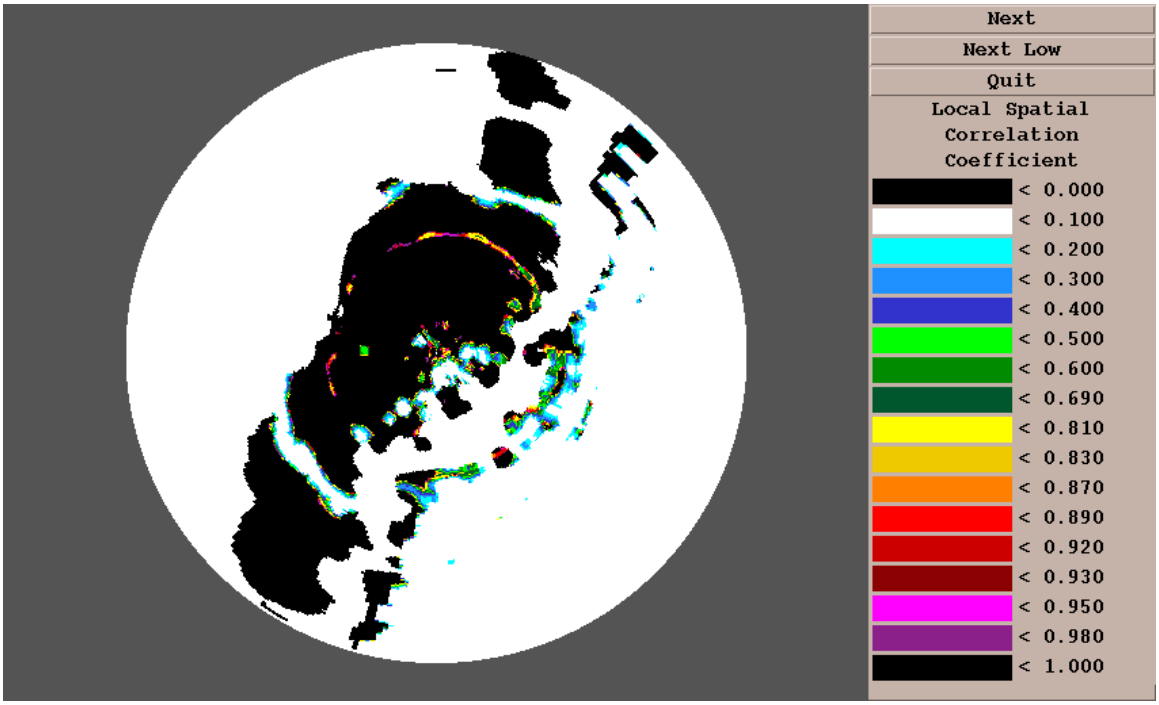

Fig 12 Spatial correlation of top height of apparent convective core, ρ_h (KINX_N04206 VS_275)

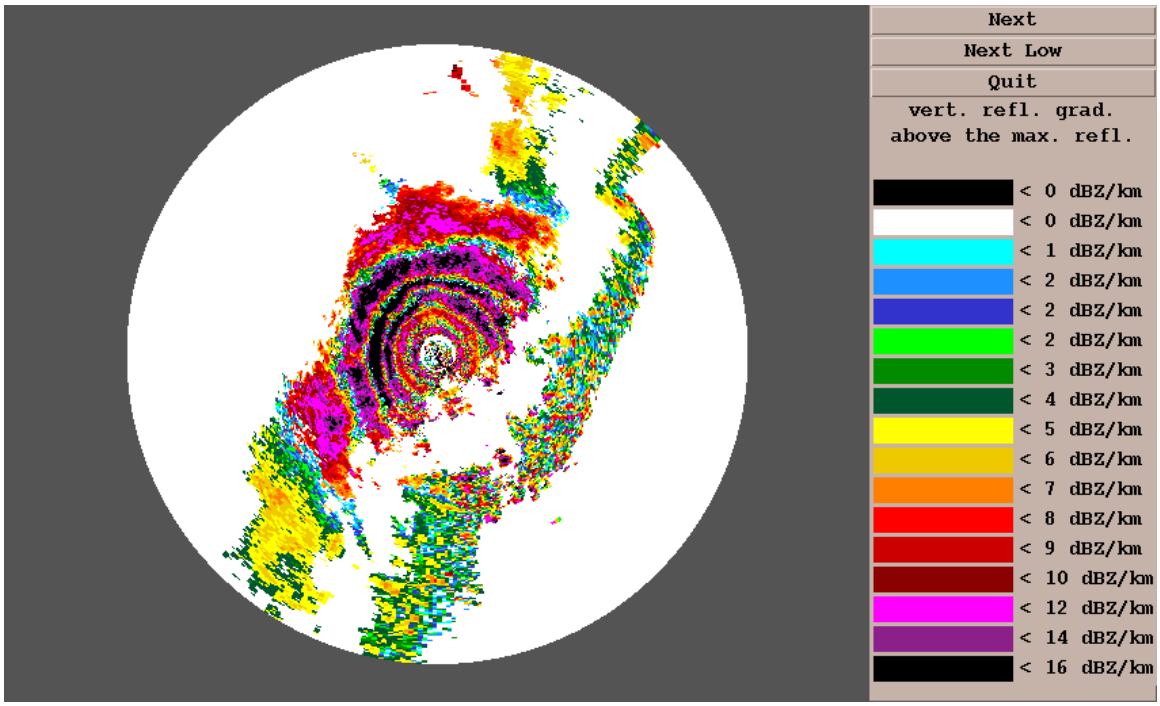

Fig 13 Reflectivity gradient in the vertical above the height of maximum reflectivity (KINX_N04206 VS_275)

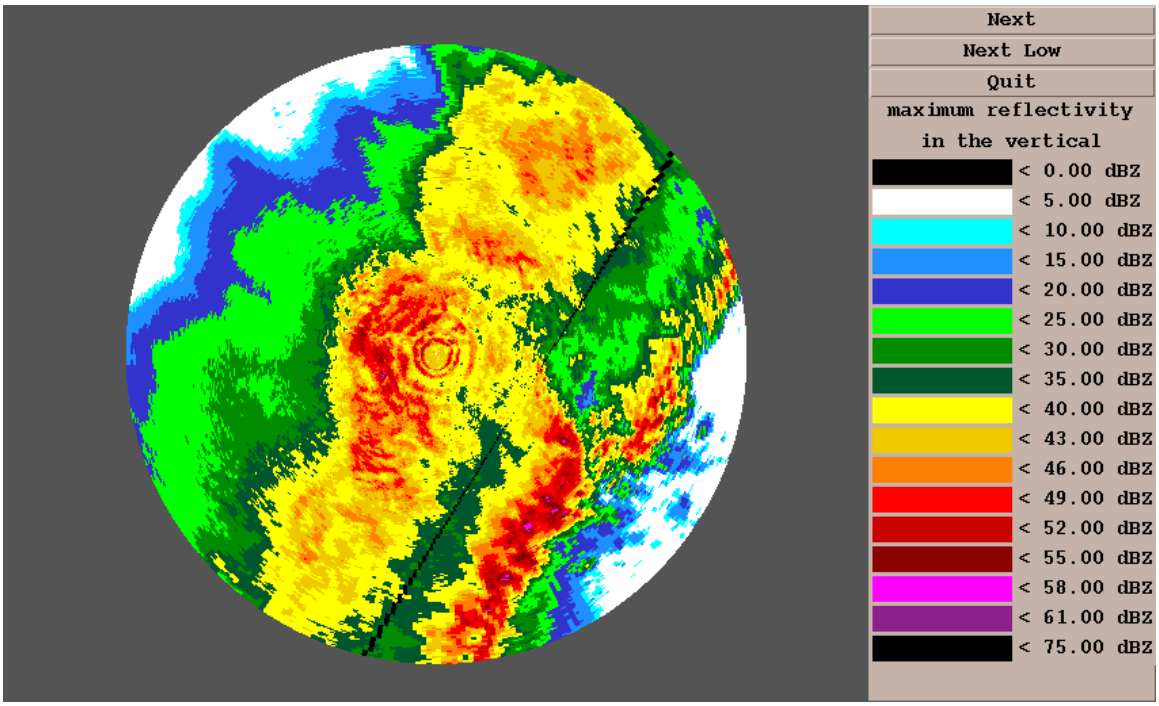

Fig 14 Maximum reflectivity in the vertical, r_x (KINX_N04206 VS_285)

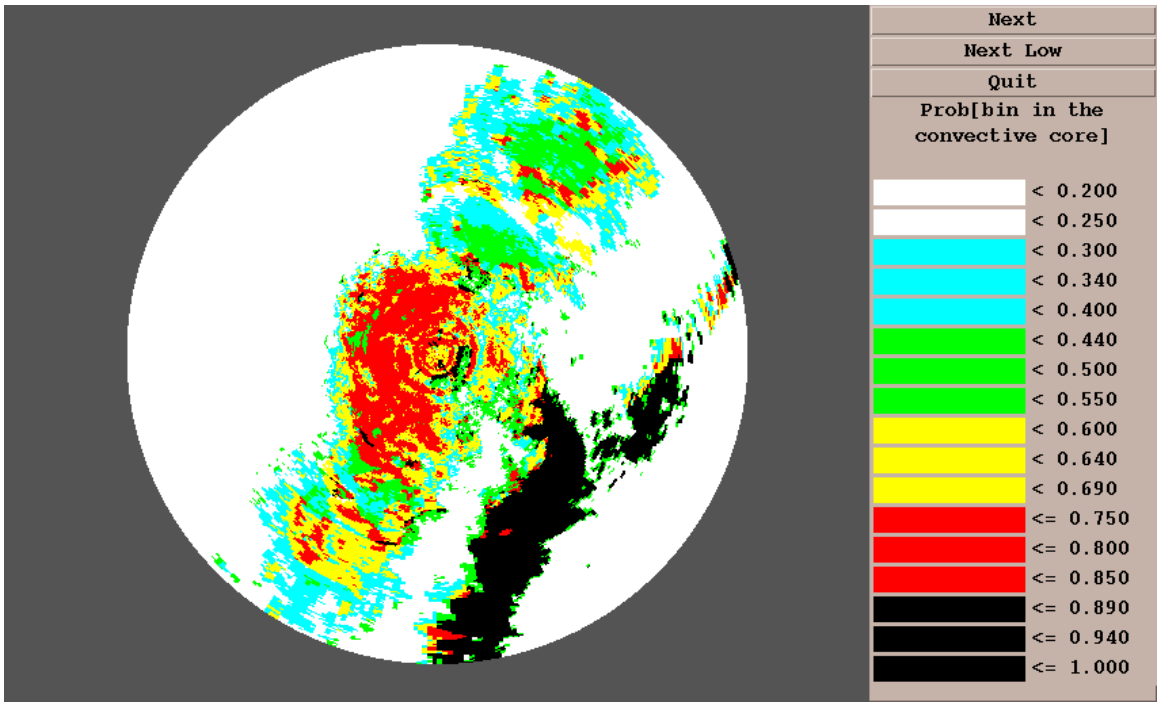

Fig 15 Prob [Bin $\in$ convective | •] (KINX_N04206 VS_285)

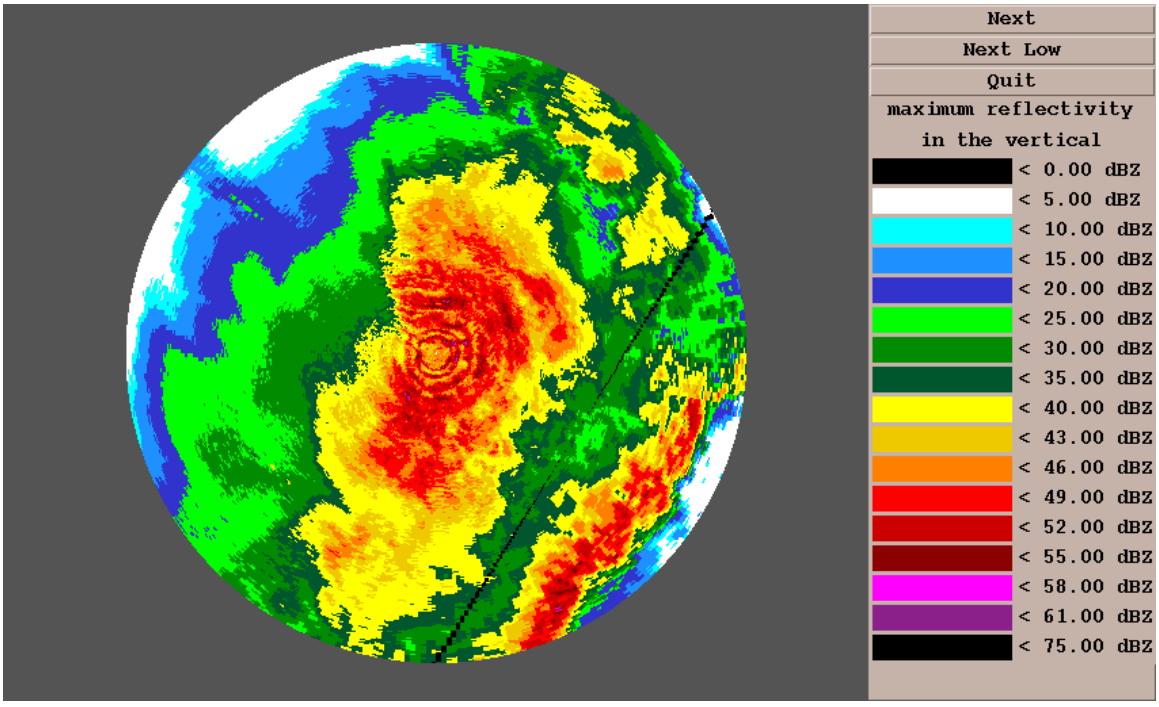

Fig 16 Maximum reflectivity in the vertical, r_x (KINX_N04206 VS_295)

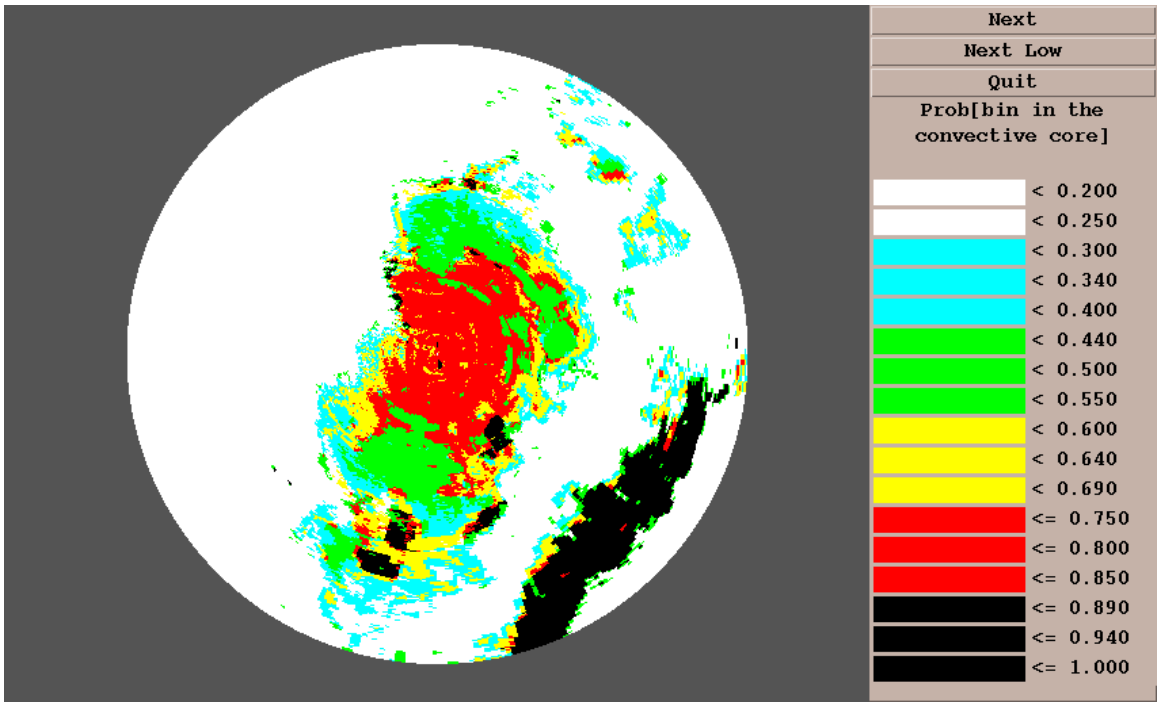

Fig 17 Prob [Bin $\in$ convective | •] (KINX_N04206 VS_295)

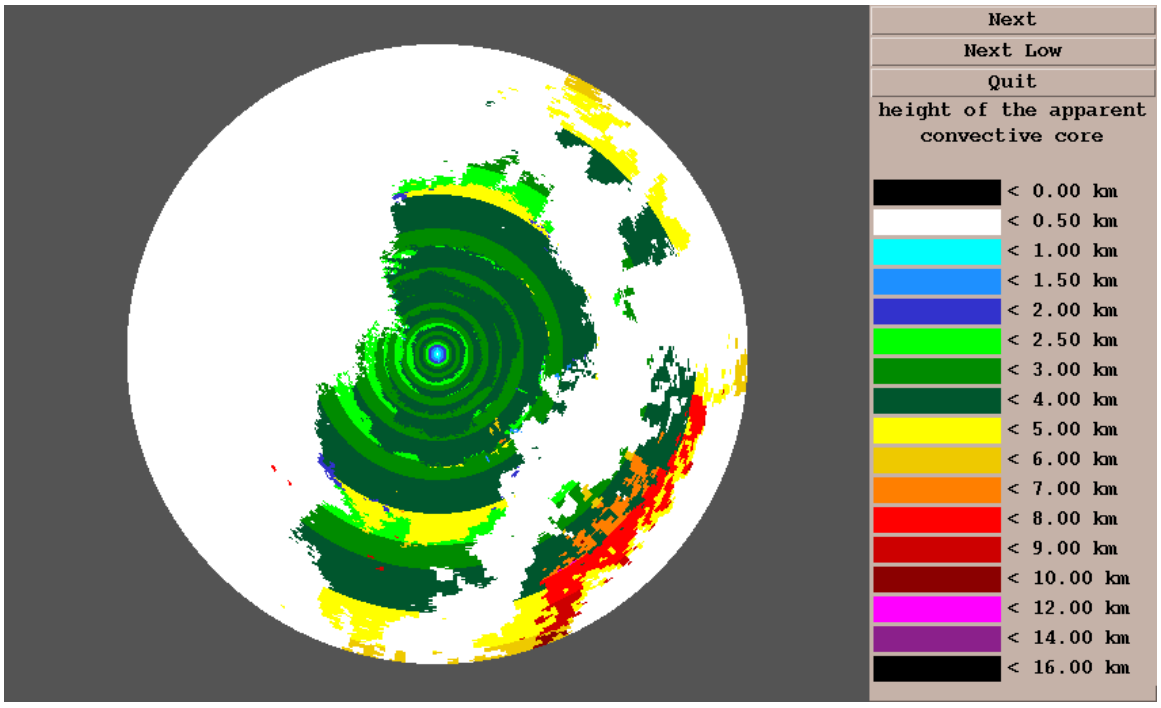

Fig 18 Top height of apparent convective core (KINX_N04206 VS_295)

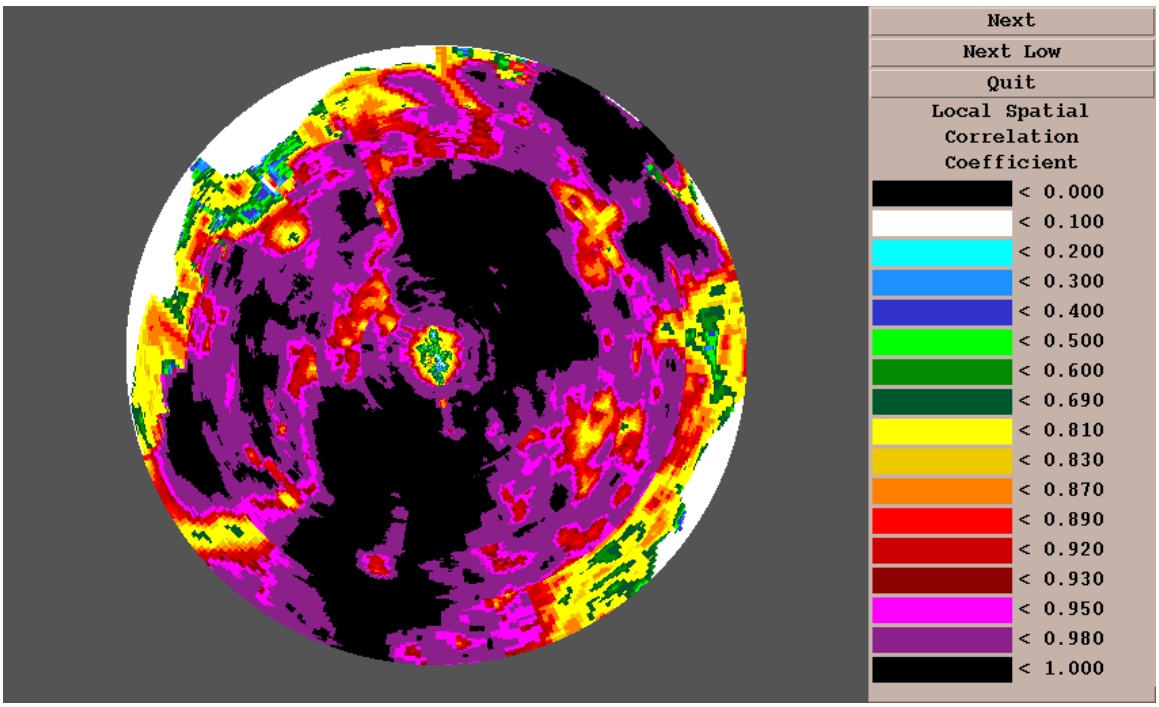

Fig 19 Vertically-averaged spatial correlation of reflectivity, ρ_r (KINX_N04206 VS_295)

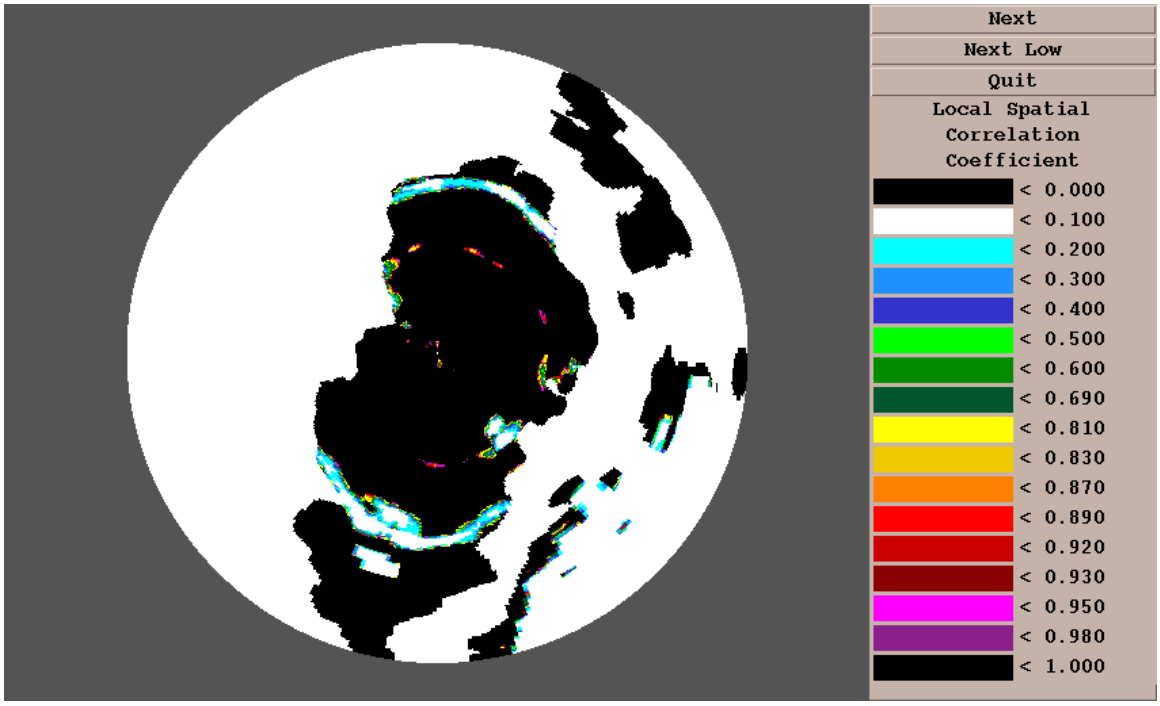

Fig 20 Spatial correlation of top height of apparent convective core, ρ_h (KINX_N04206 VS_295)

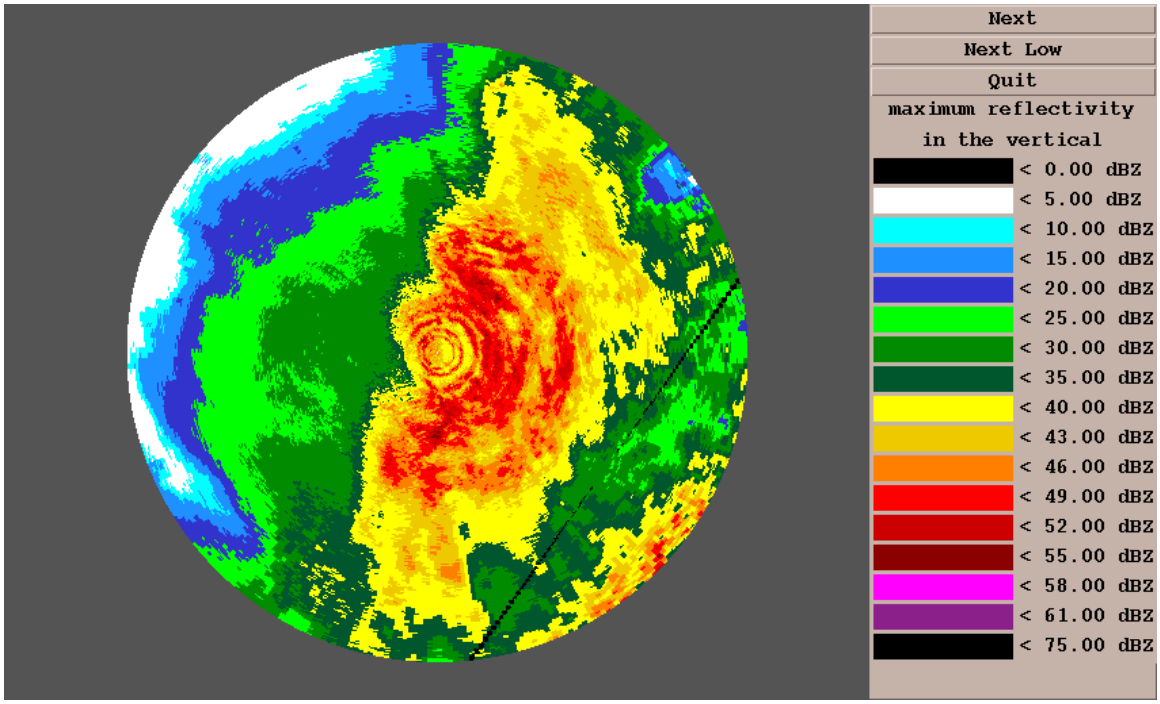

Fig 21 Maximum reflectivity in the vertical, r_x (KINX_N04206 VS_305)

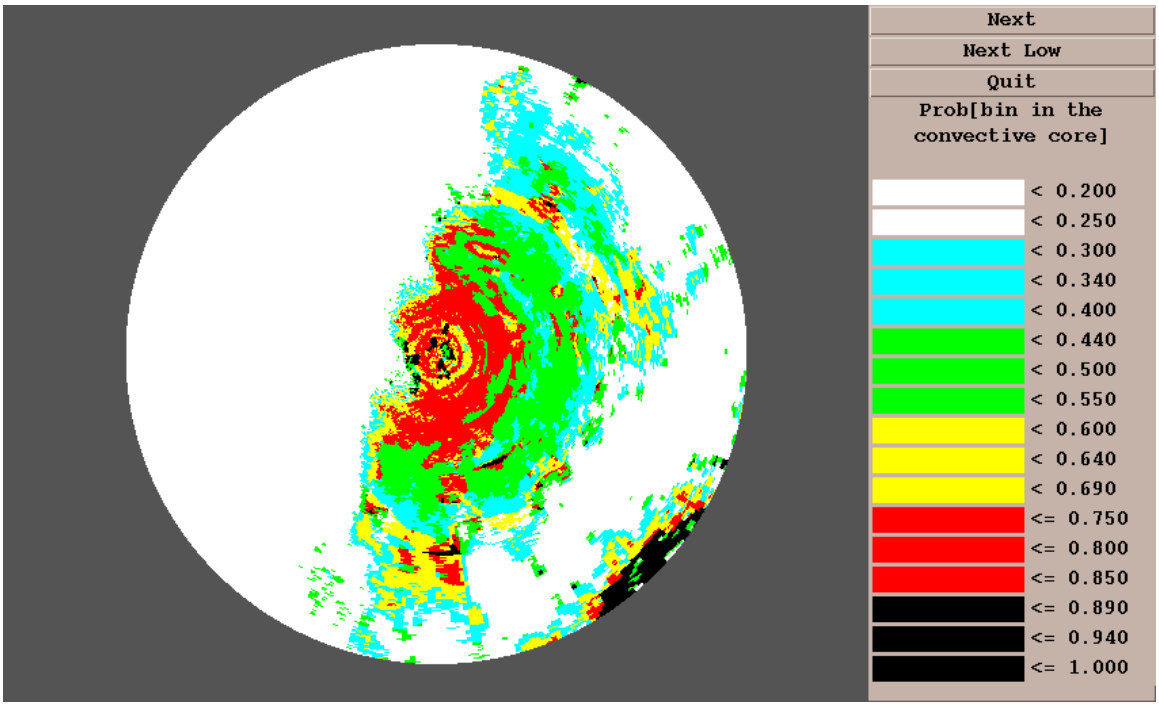

Fig 22 Prob [Bin $\in$ convective | •] (KINX_N04206 VS_305)

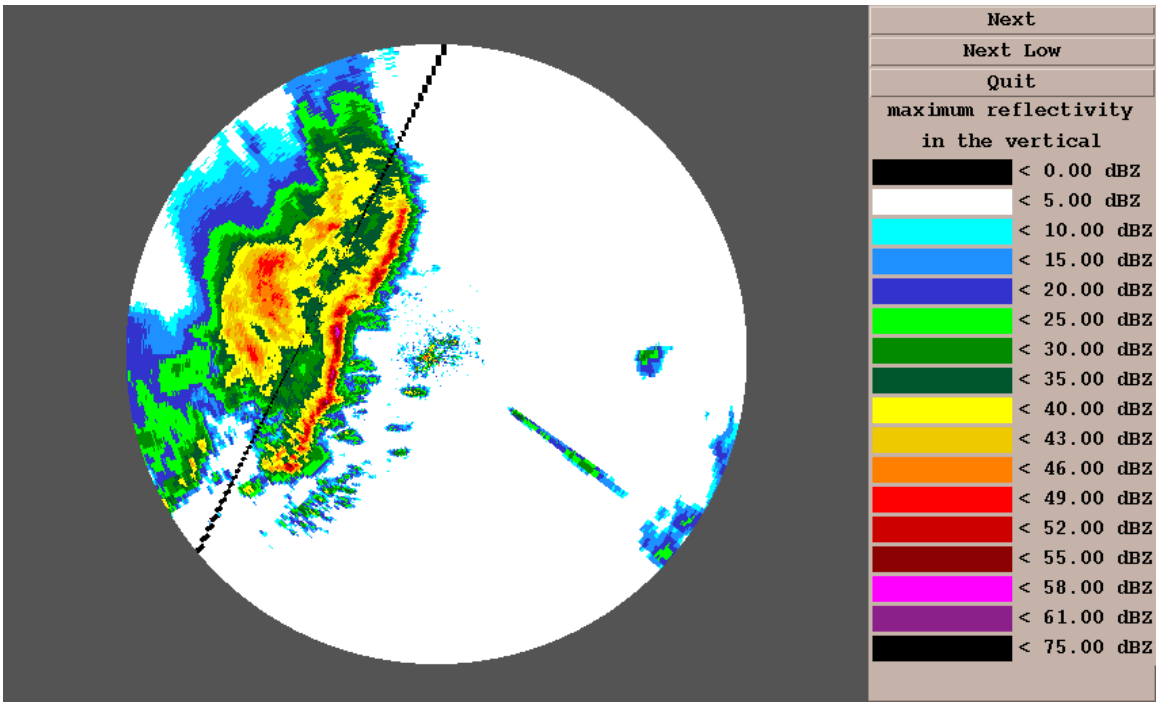

Fig 23 Maximum reflectivity in the vertical, r_x (KAMA_N04248 VS_105)

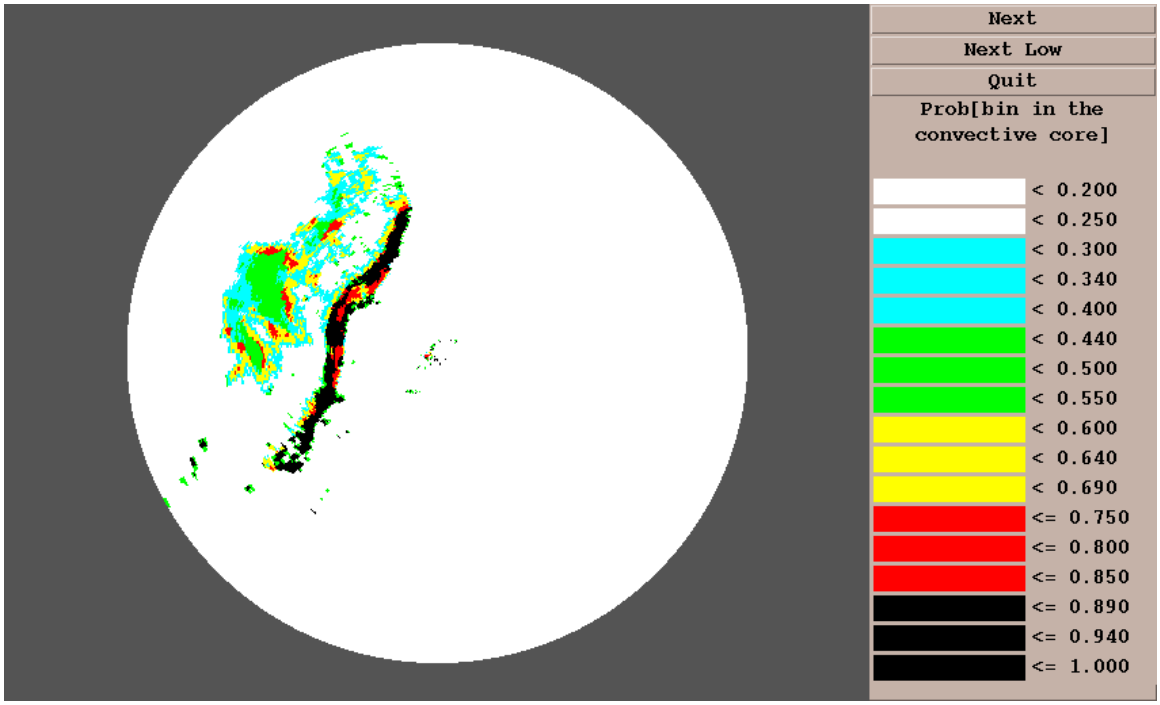

Fig 24 Prob [Bin $\in$ convective | •] (KAMA_N04248 VS_105)

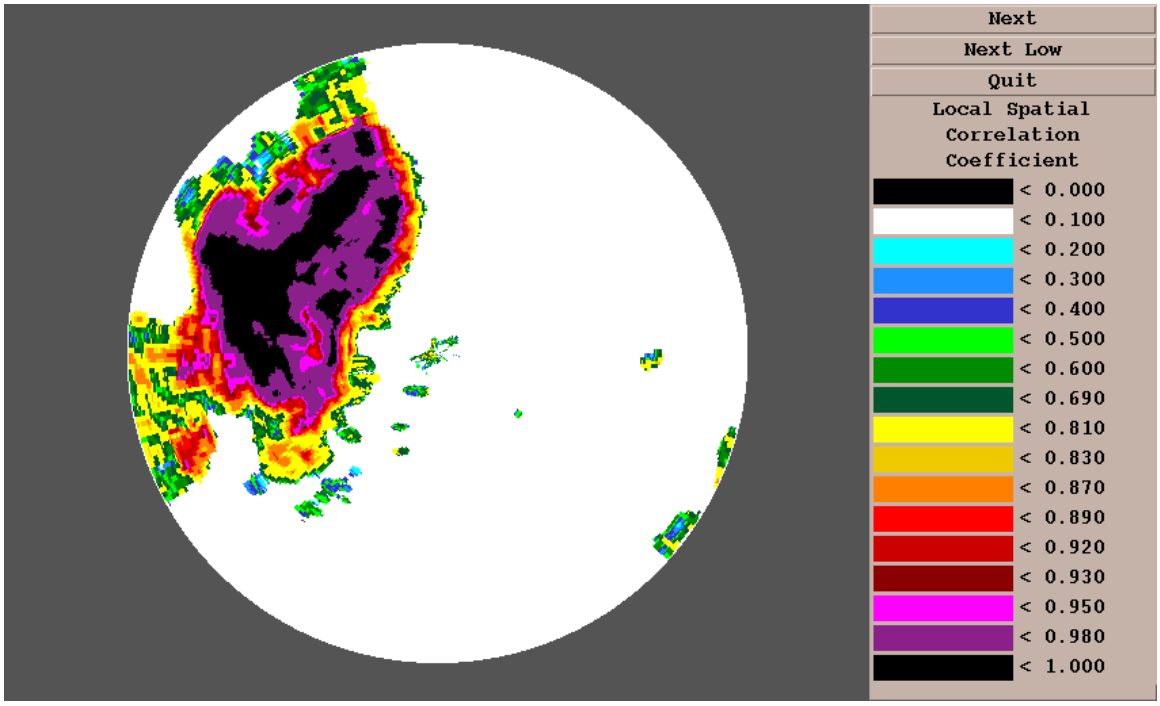

Fig 25 Vertically-averaged spatial correlation of reflectivity, ρ_r (KAMA_N04248 VS_105)

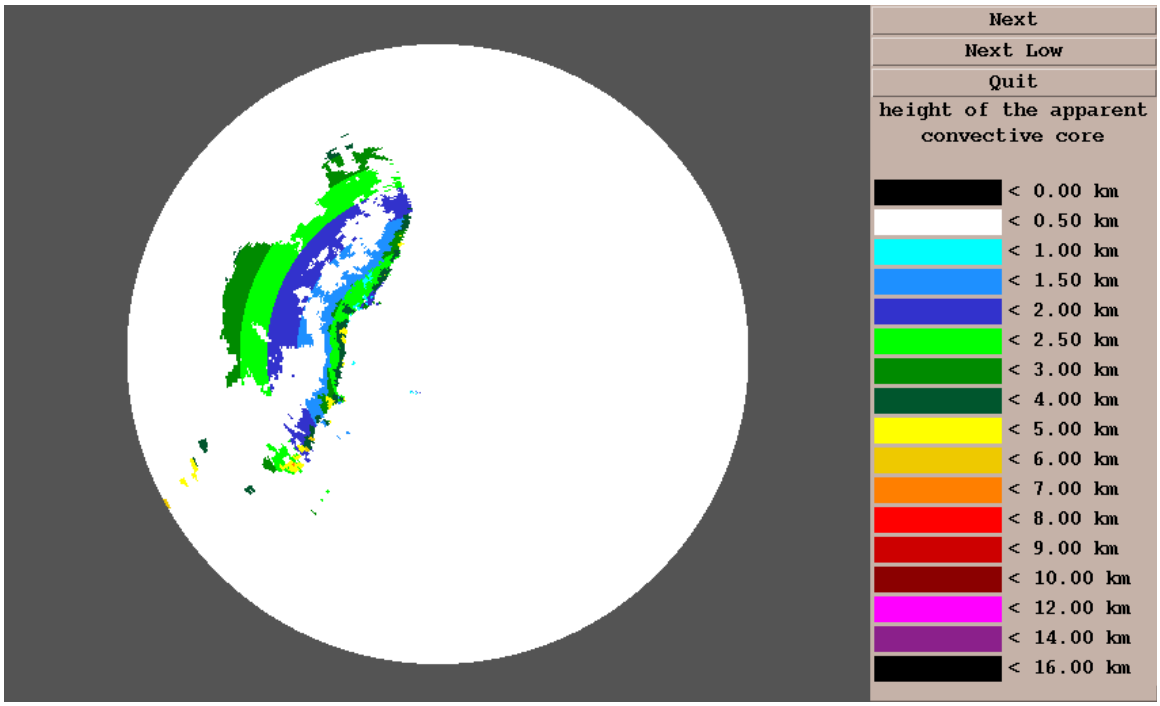

Fig 26 Top height of apparent convective core (KAMA_N04248 VS_105)

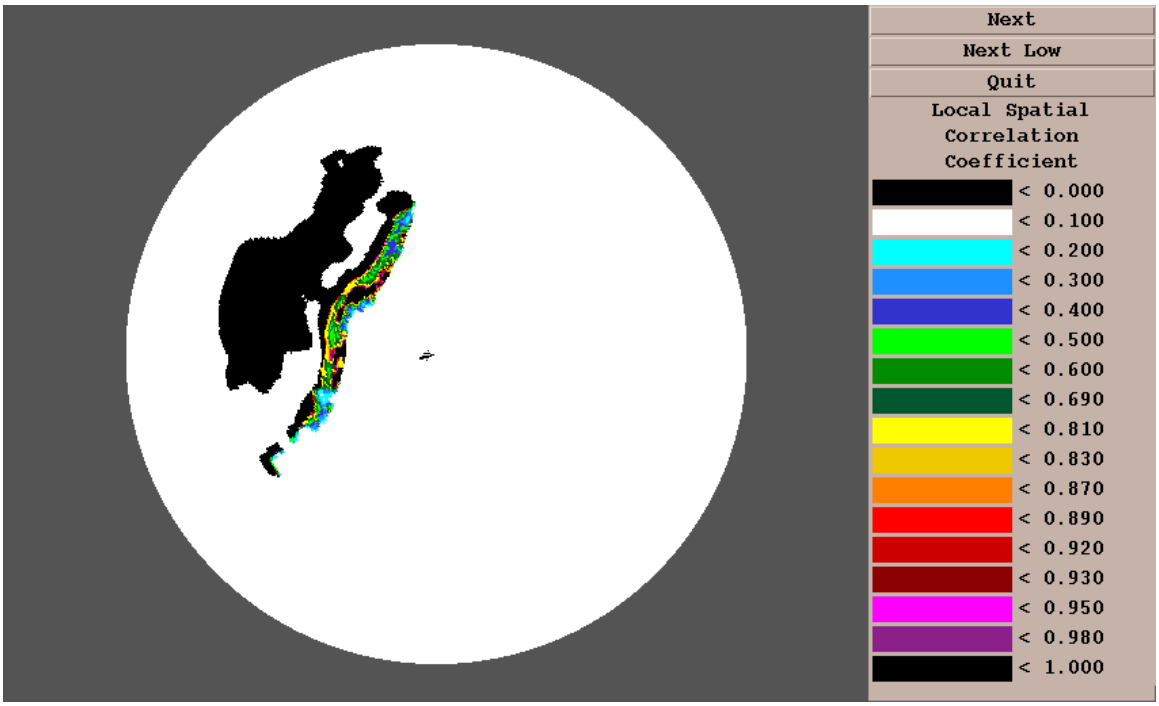

Fig 27 Spatial correlation of top height of apparent convective core, ρ_h (KAMA_N04248 VS_105)

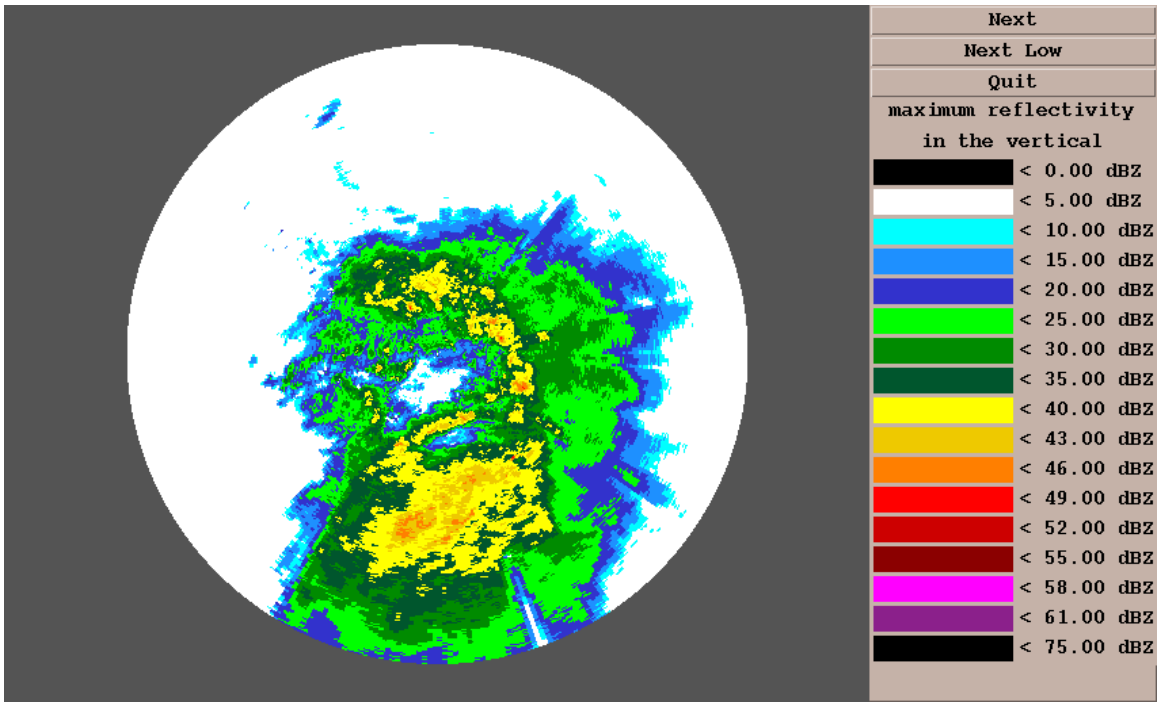

Fig 28 Maximum reflectivity in the vertical, r_x (KATX_N10814 VS_16)

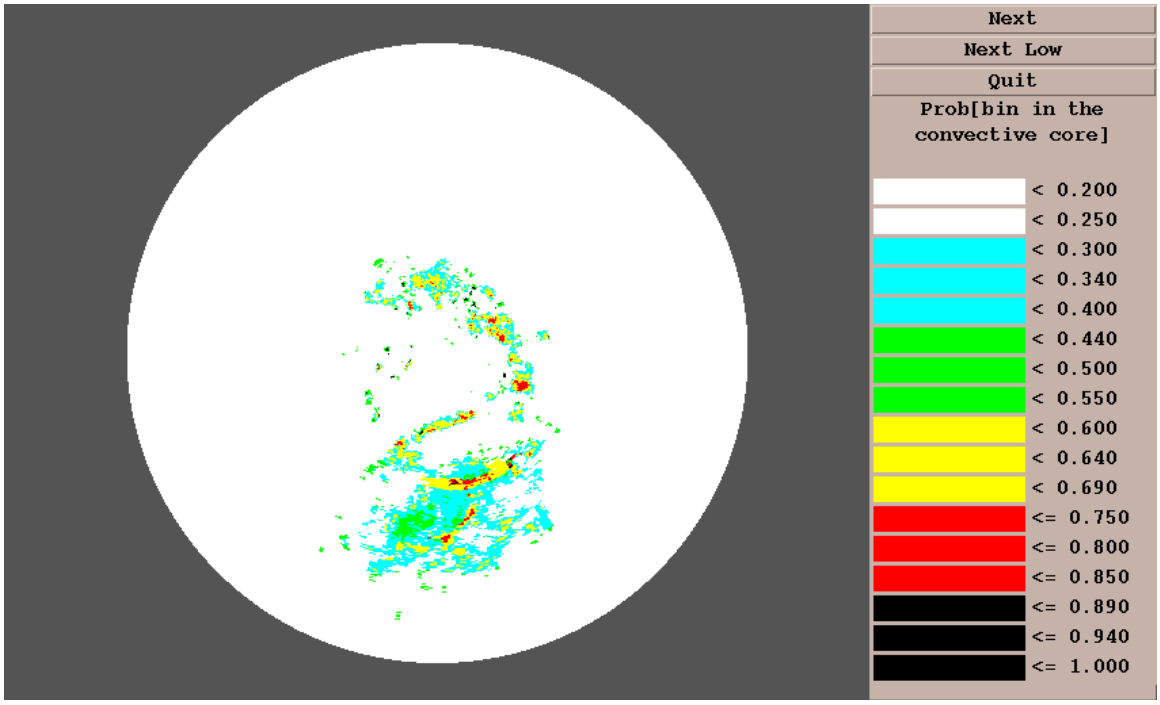

Fig 29 Prob [Bin $\in$ convective | •] (KATX_N10814 VS_16)

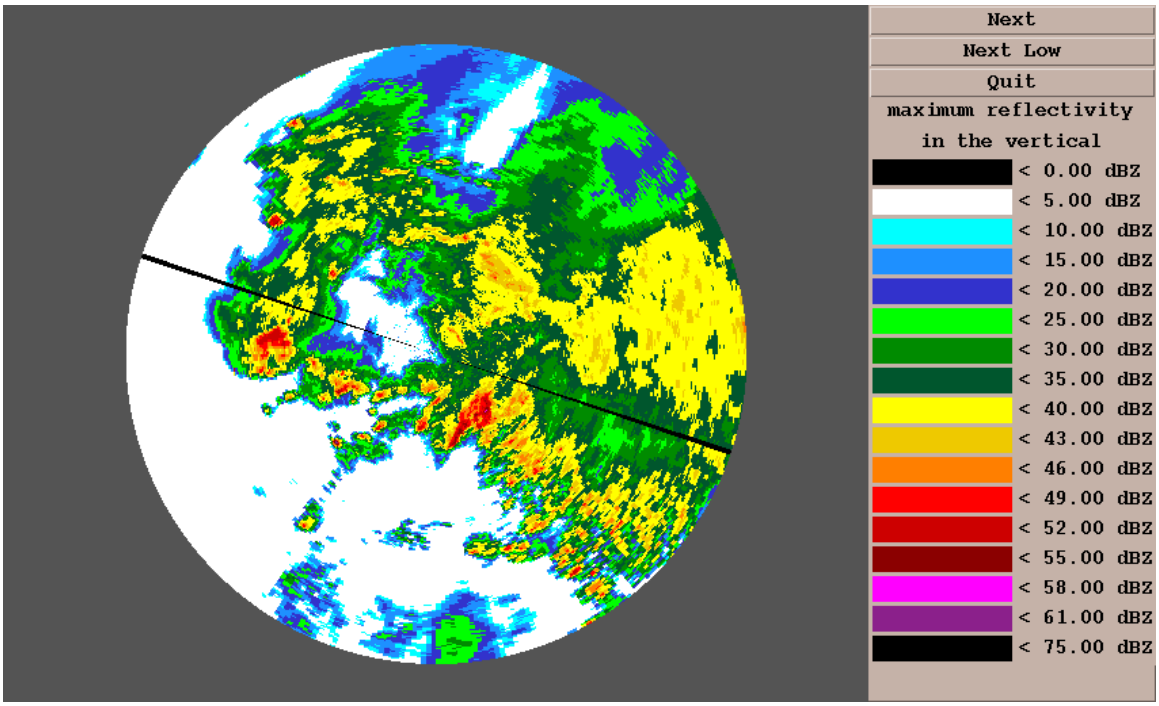

Fig 30 Maximum reflectivity in the vertical, r_x (KDDC_N01158 VS_259)

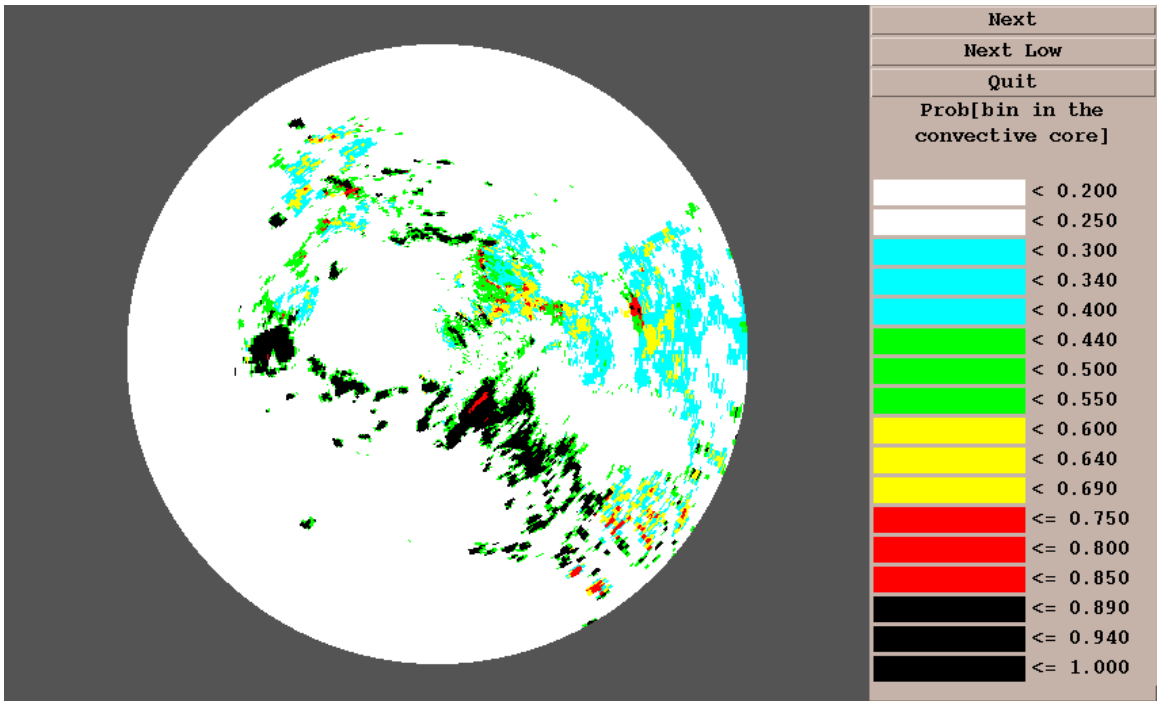

Fig 31 Prob [Bin $\in$ convective | •] (KDDC_N01158 VS_259)

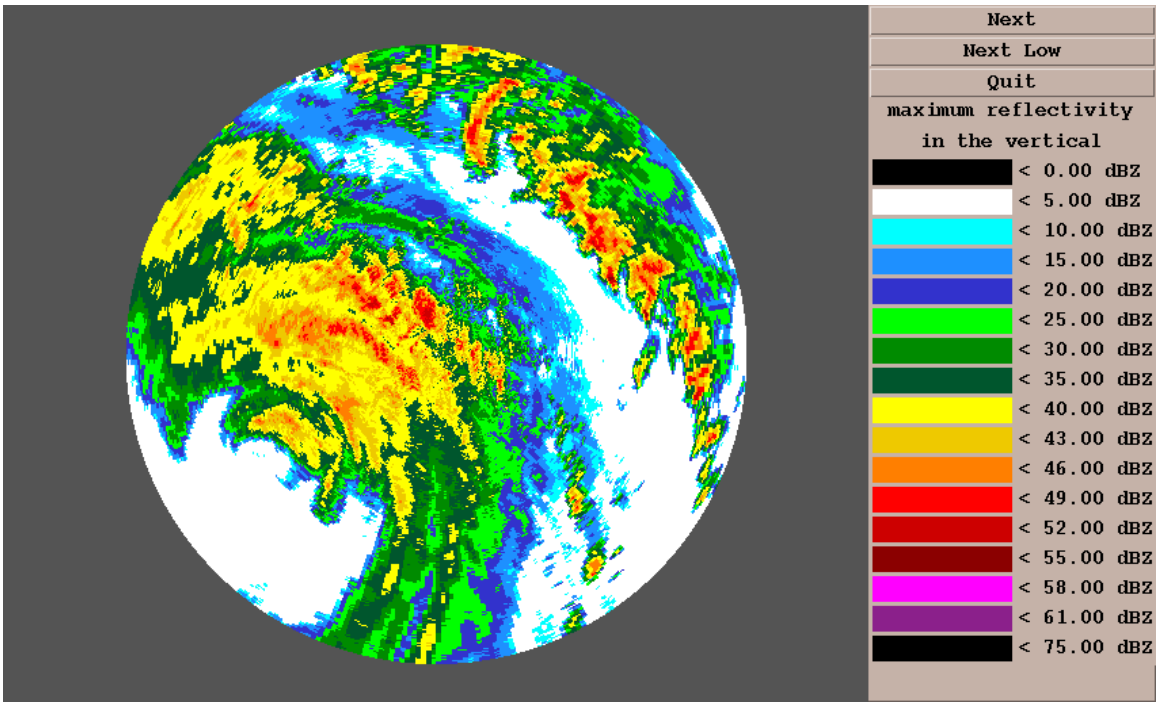

Fig 32 Maximum reflectivity in the vertical, r_x (KEVX_N09652 VS_191)

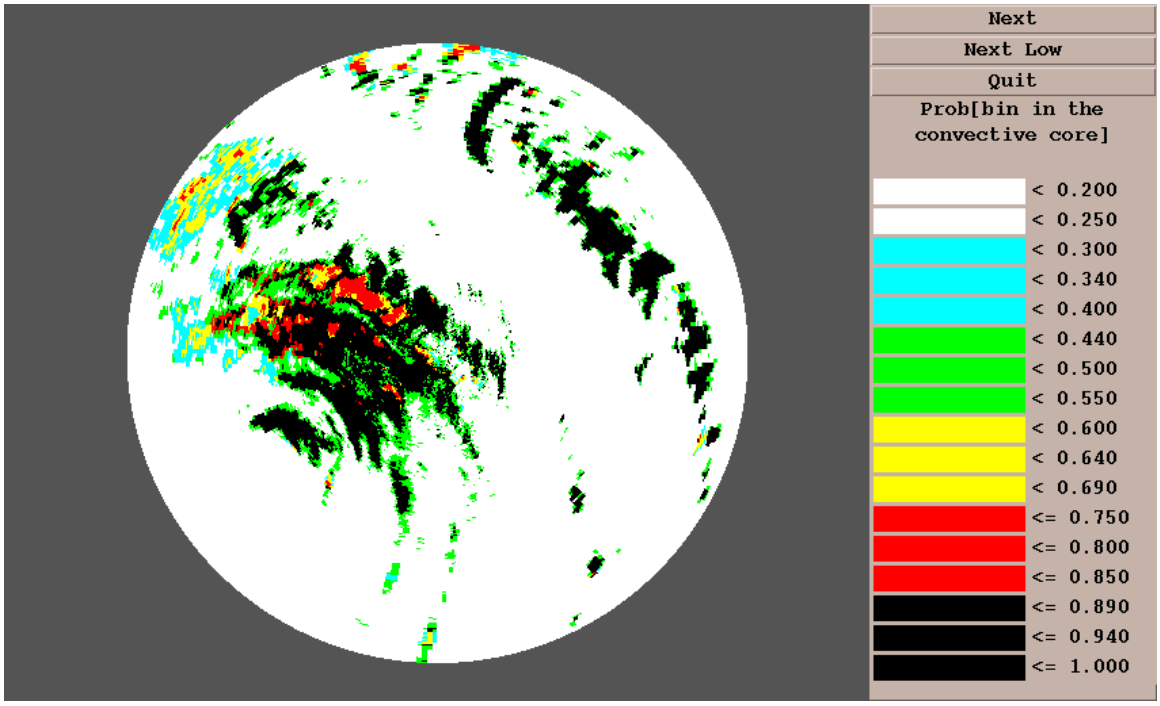

Fig 33 Prob [Bin $\in$ convective | •] (KEVX_N09652 VS_191)

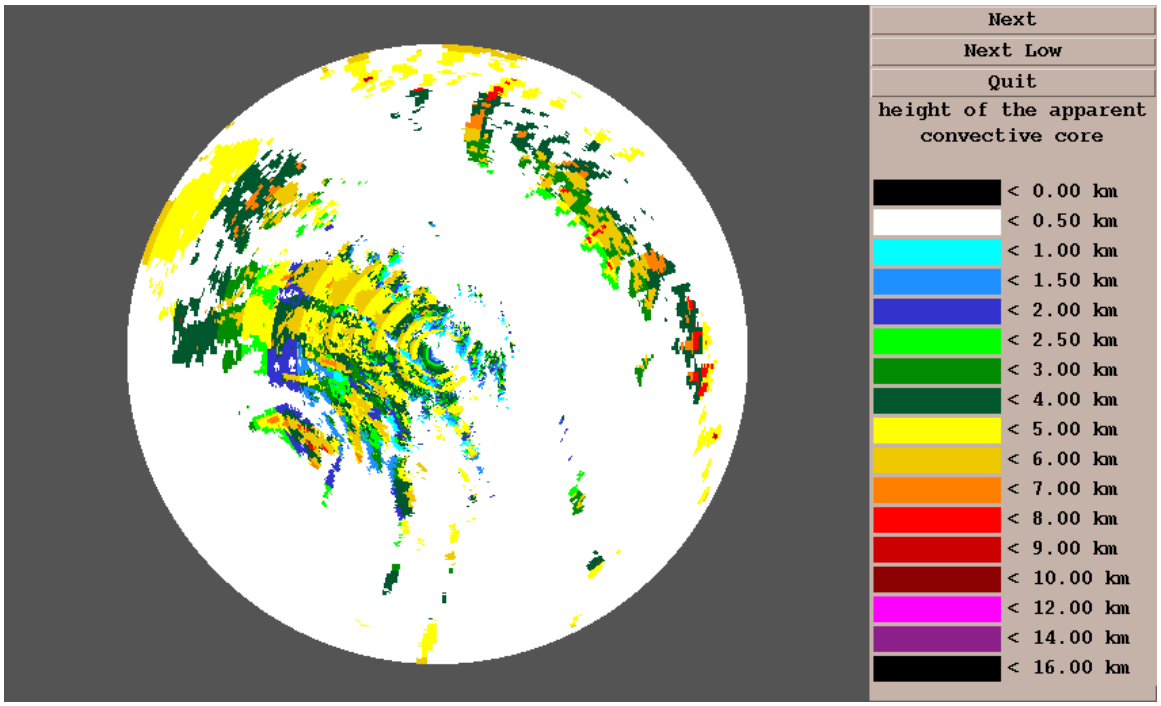

Fig 34 Top height of apparent convective core (KEVX_N09652 VS_191)

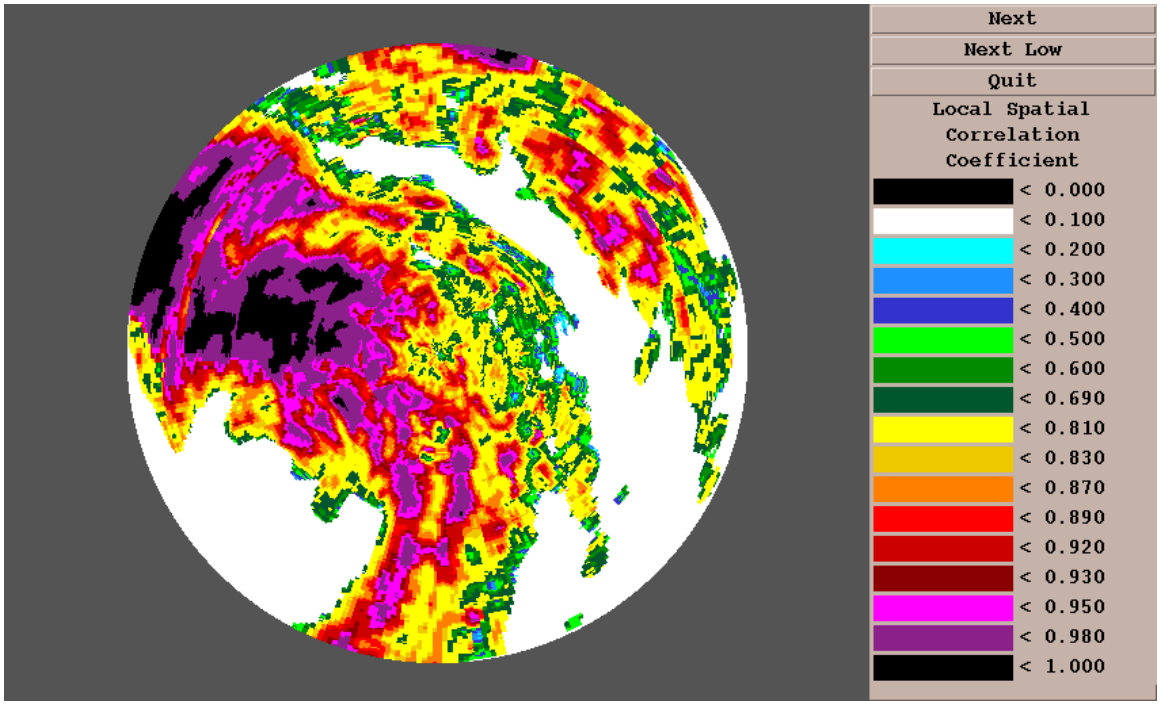

Fig 35 Vertically-averaged spatial correlation of reflectivity, ρ_r (KEVX_N09652 VS_191)

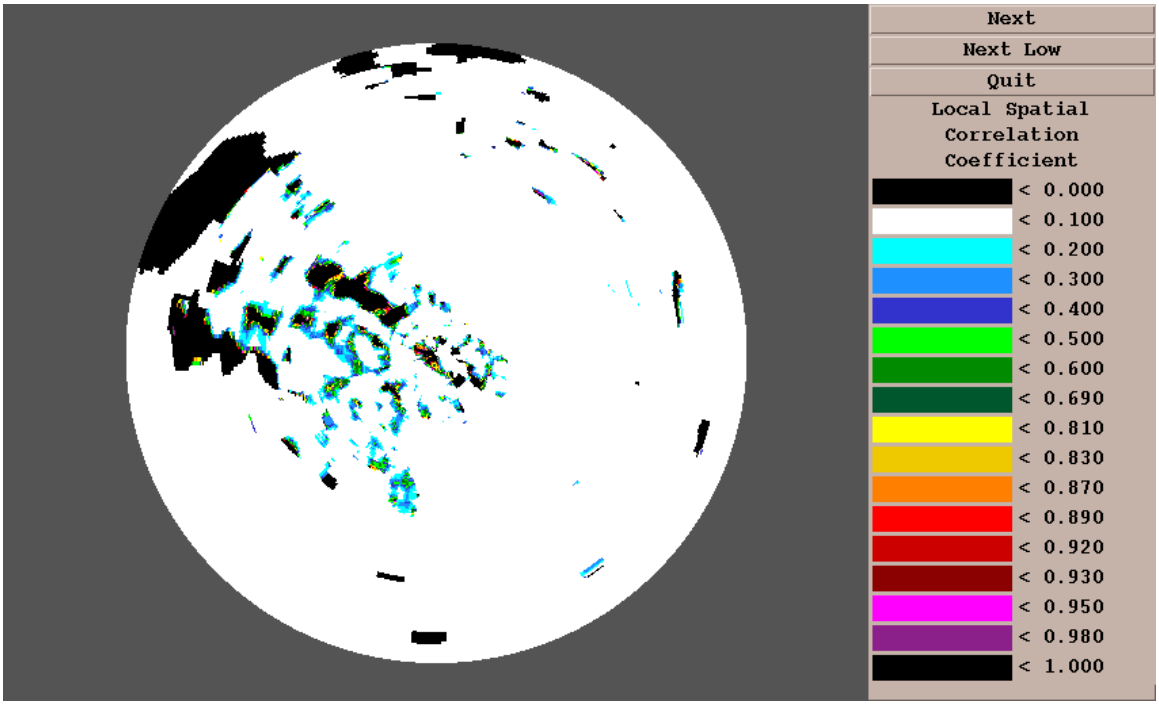

Fig 36 Spatial correlation of height of apparent convective core, ρ_h (KEVX_N09652 VS_191)

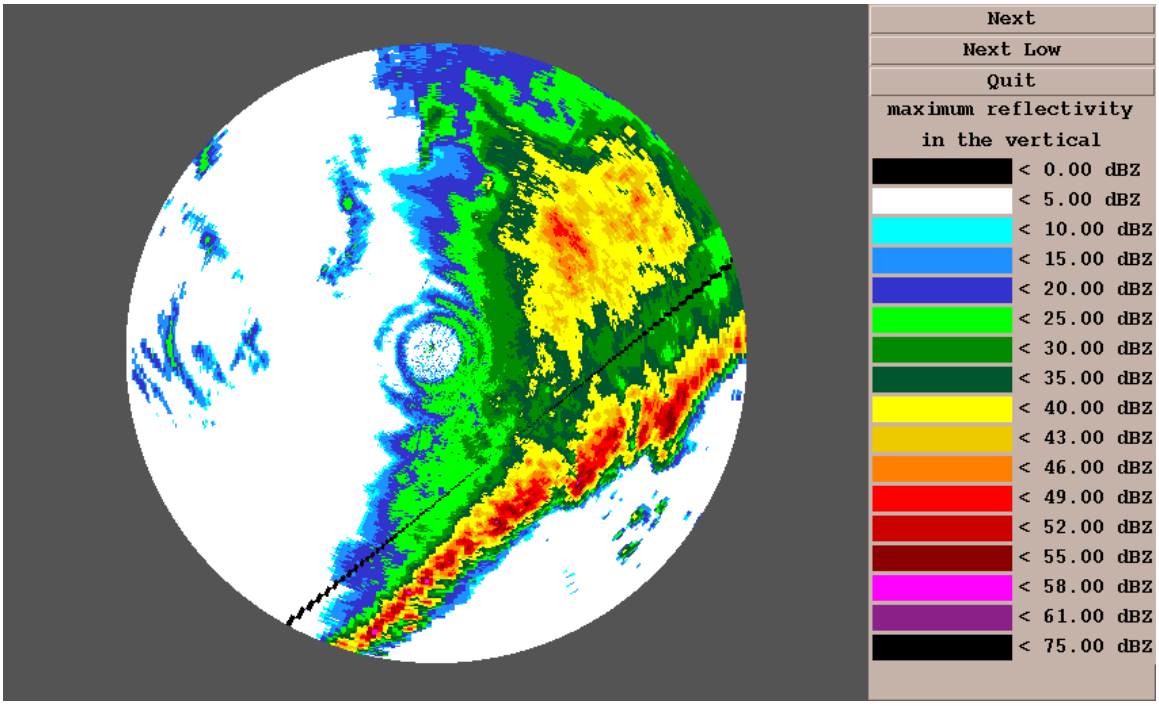

Fig 37 Maximum reflectivity in the vertical, r_x (KFDR_N01114 VS_80)

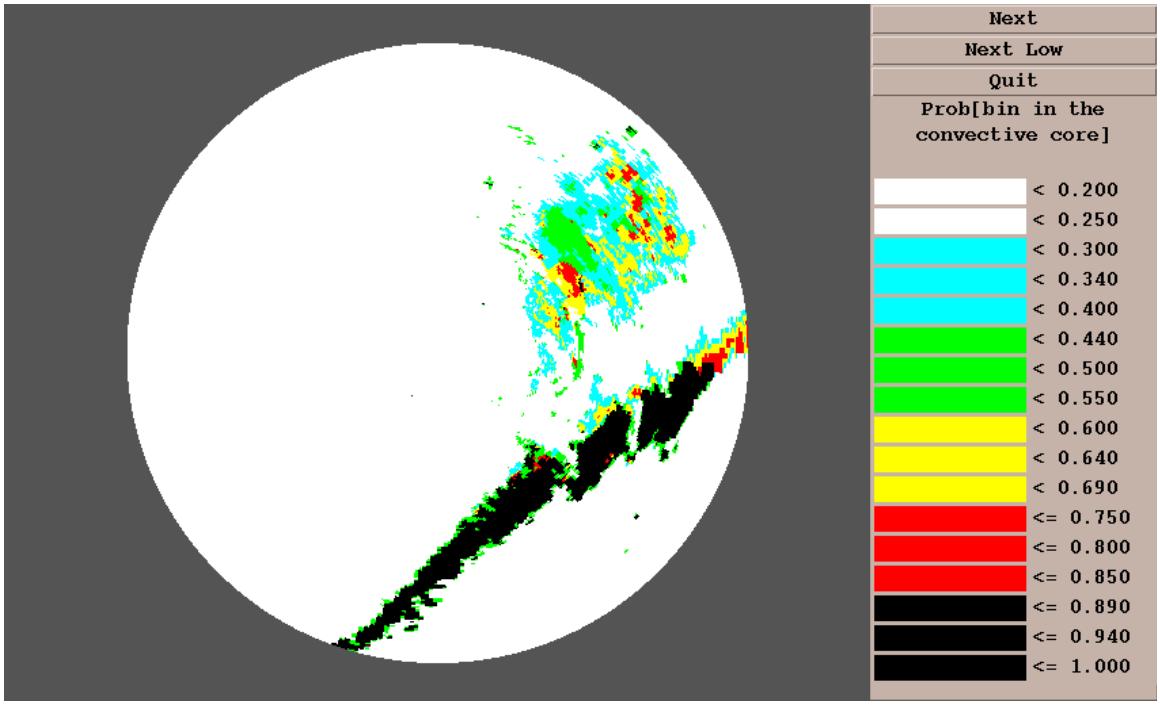

Fig 38 Prob [Bin $\in$ convective | •] (KFDR_N01114 VS_80)

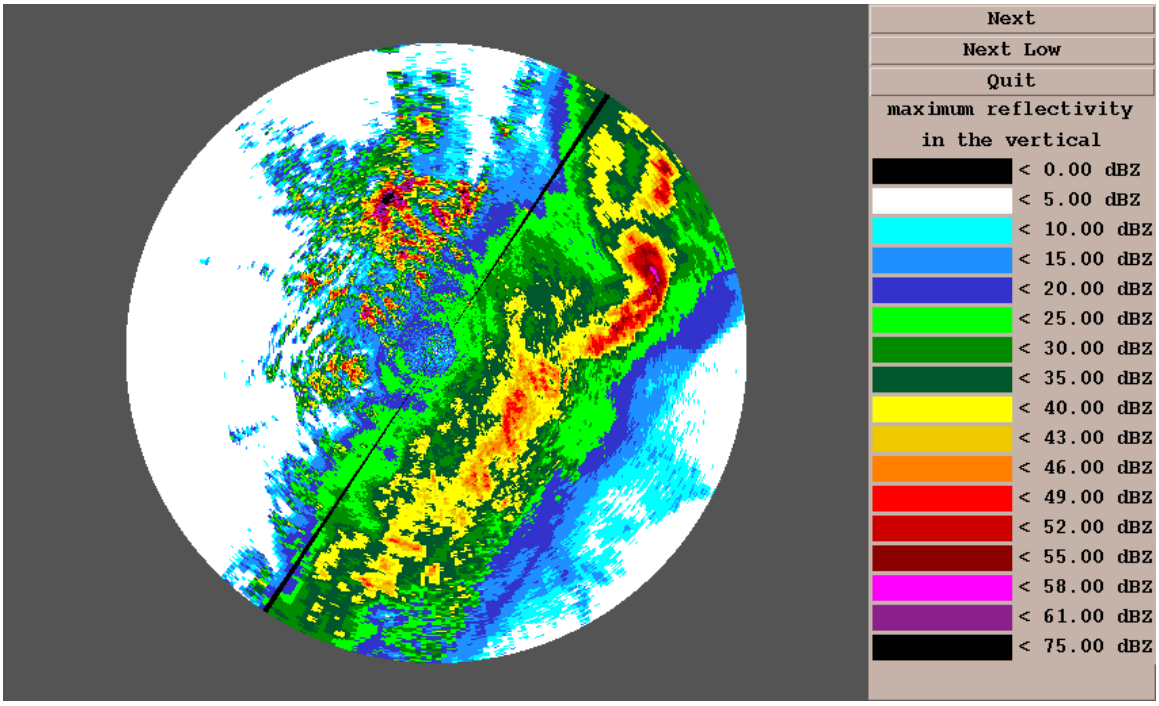

Fig 39 Maximum reflectivity in the vertical, r_x (KFWS_N02983 VS_370)

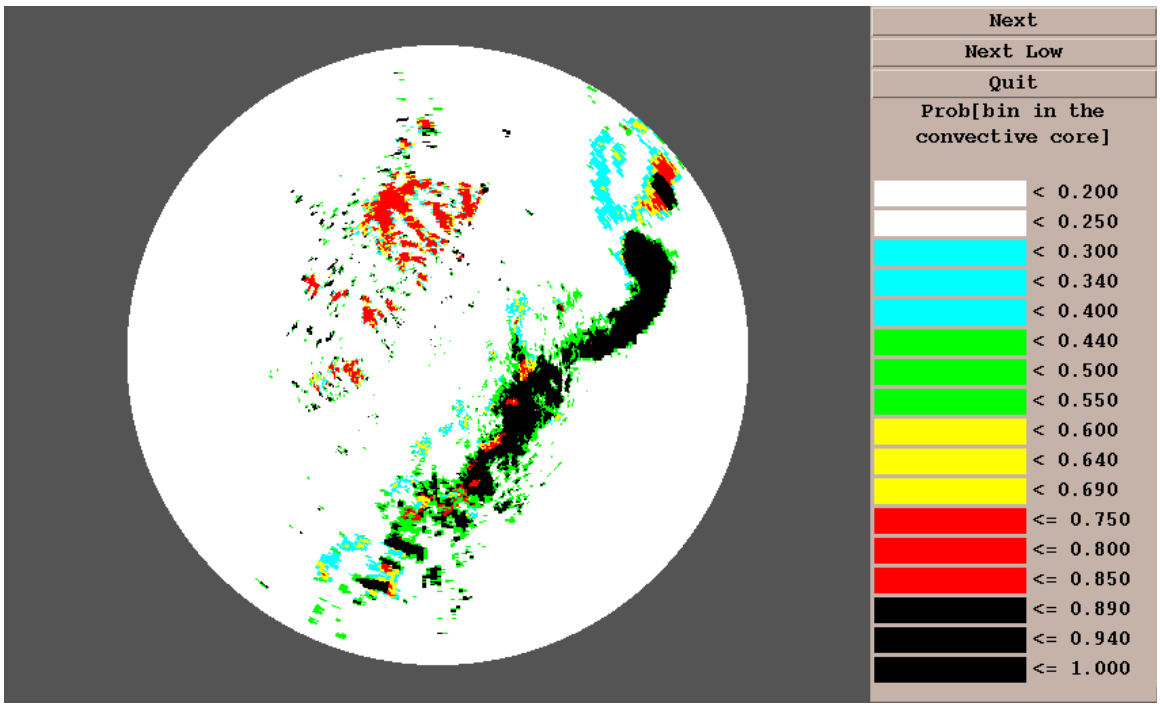

Fig 40 Prob [Bin $\in$ convective | •] (KFWS_N02983 VS_370)

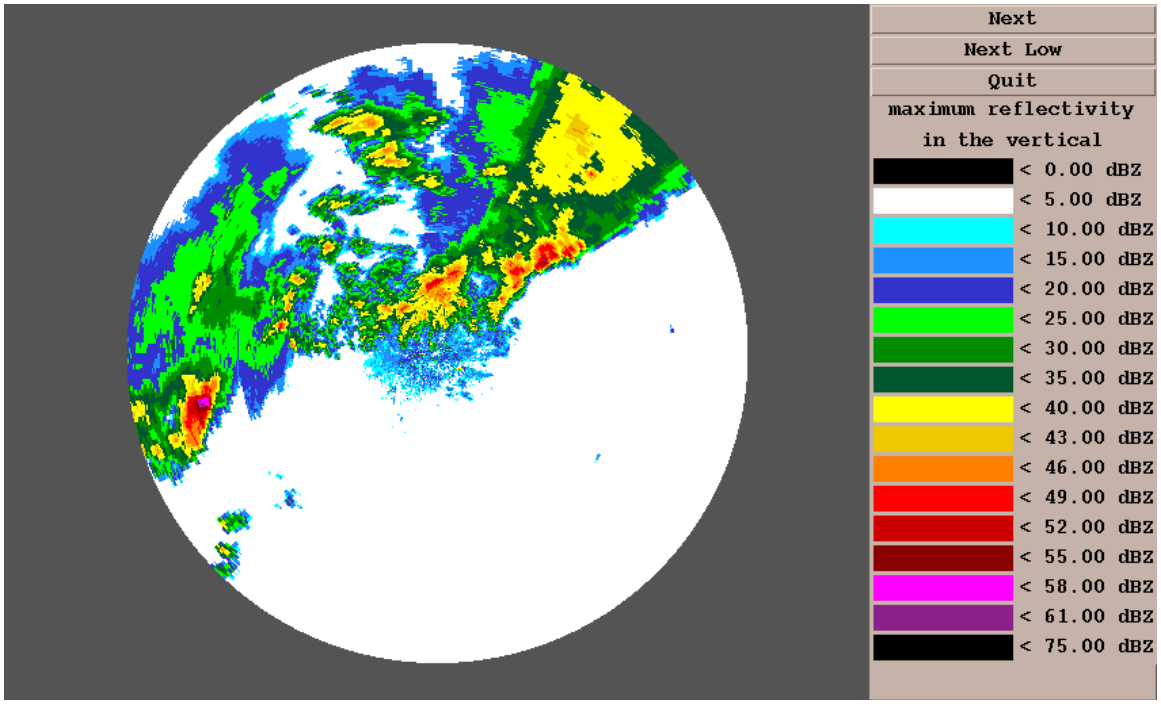

Fig 41 Maximum reflectivity in the vertical, r_x (KHGX_N02961 VS_60)

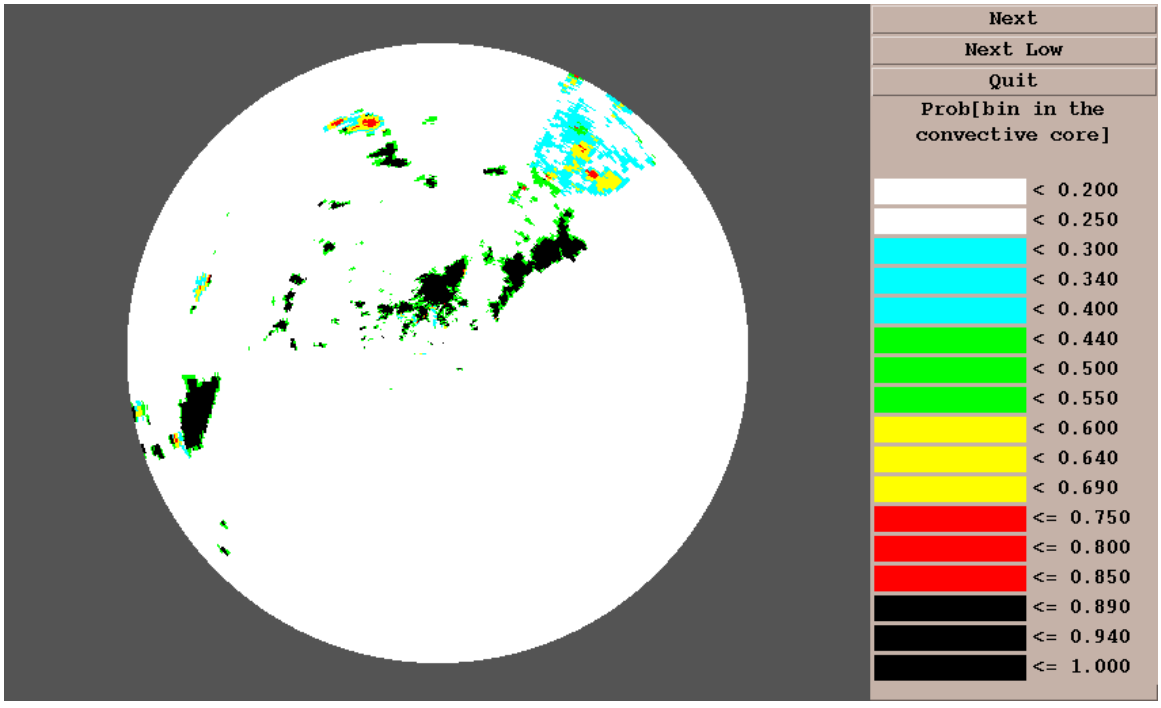

Fig 42 Prob [Bin $\in$ convective | •] (KHGX_N02961 VS_60)

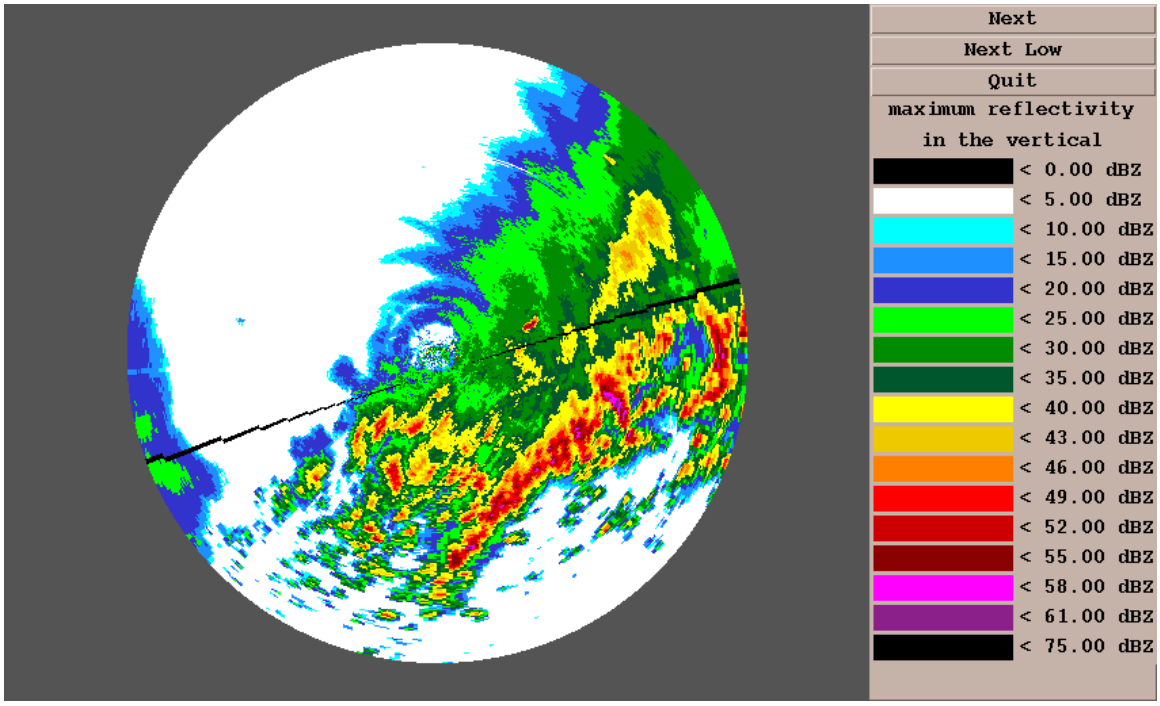

Fig 43 Maximum reflectivity in the vertical, r_x (KICT_N02075 VS_153)

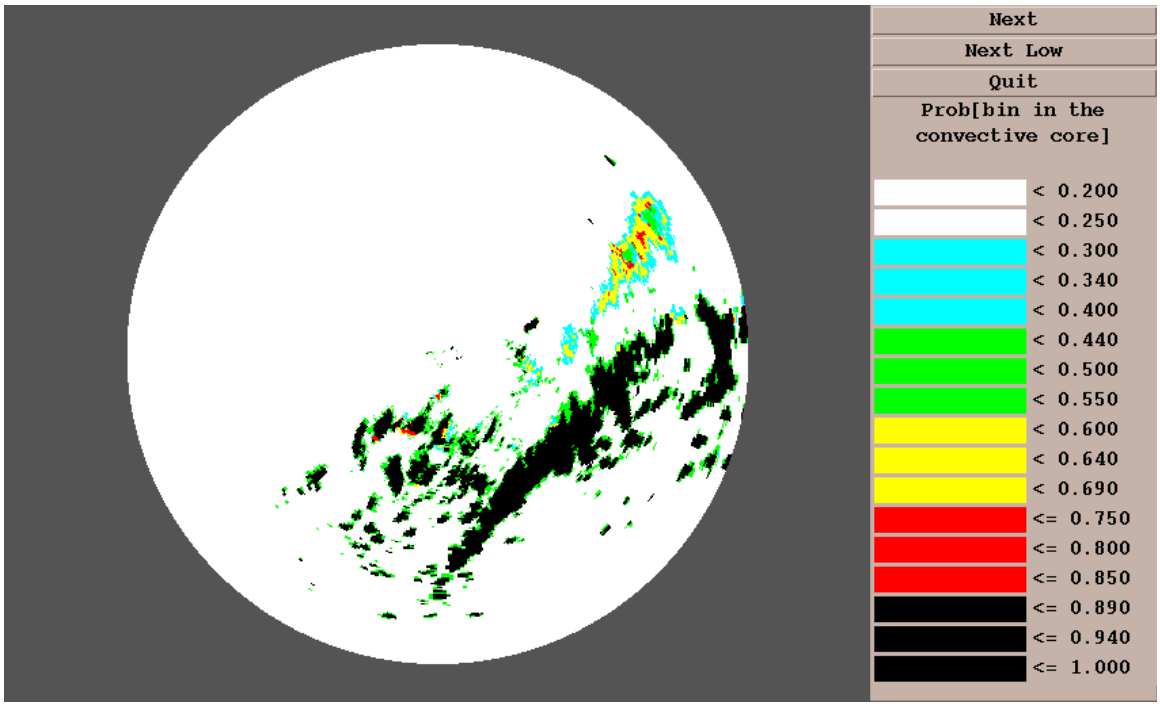

Fig 44 Prob [Bin $\in$ convective | •] (KICT_N02075 VS_153)

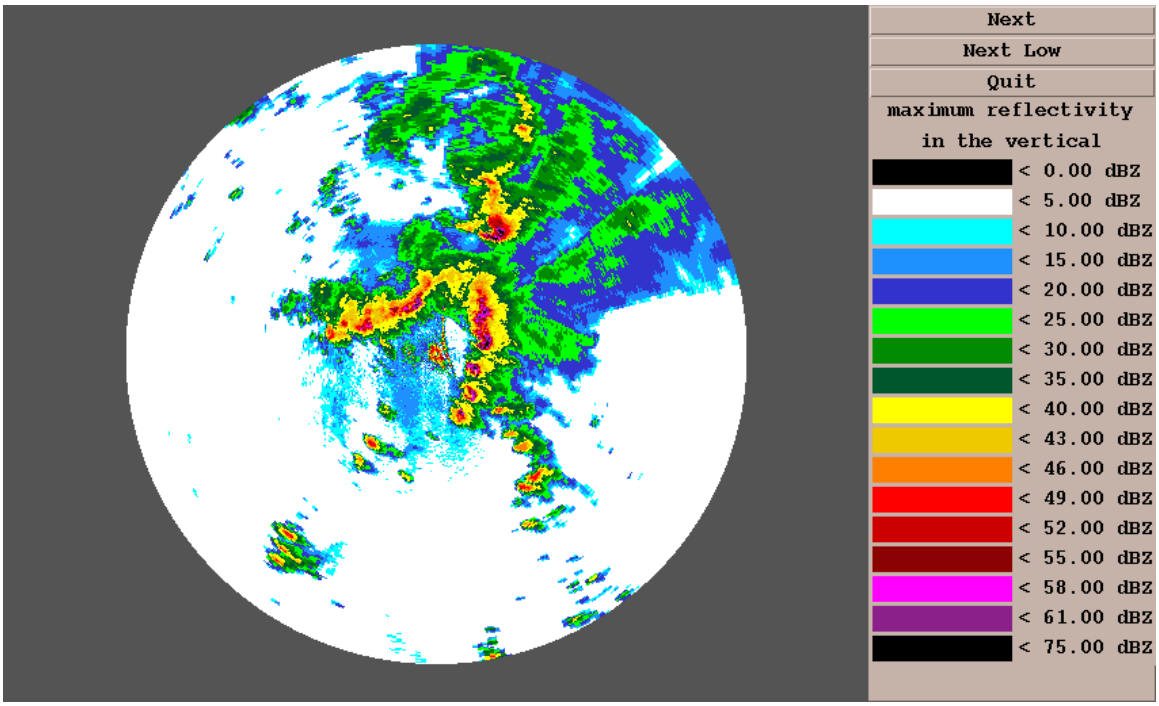

Fig 45 Maximum reflectivity in the vertical, r_x (KMLB_A20054 VS_80)

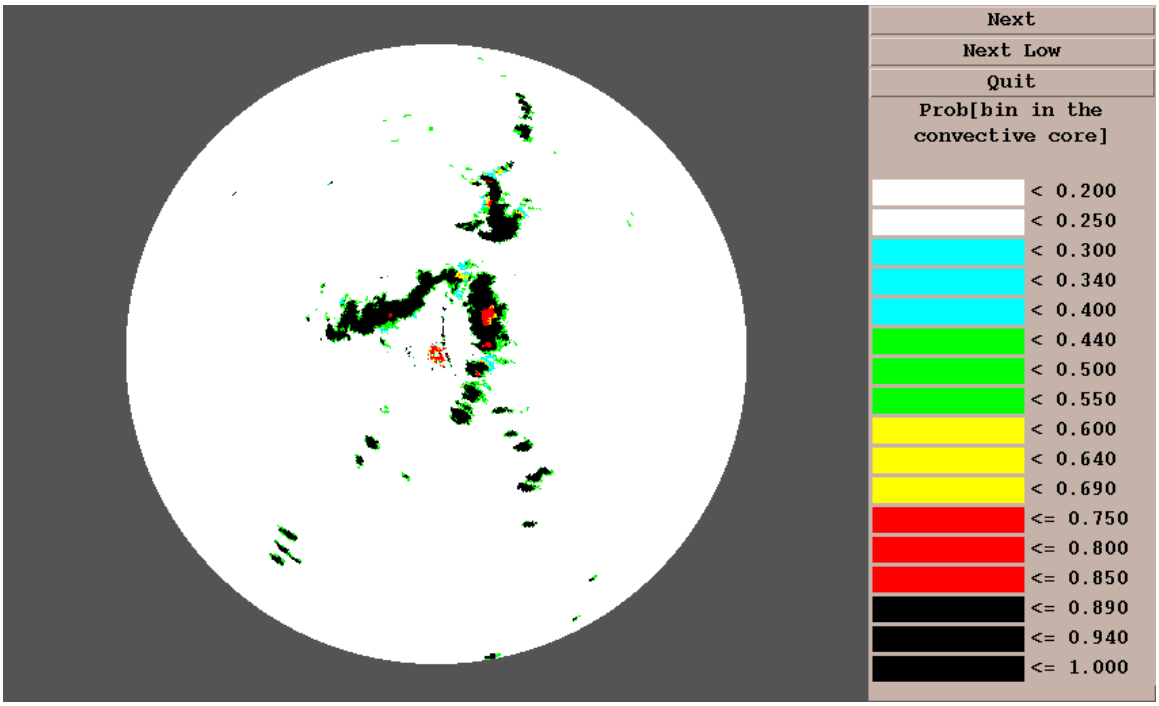

Fig 46 Prob [Bin $\in$ convective | •] (KMLB_A20054 VS_80)

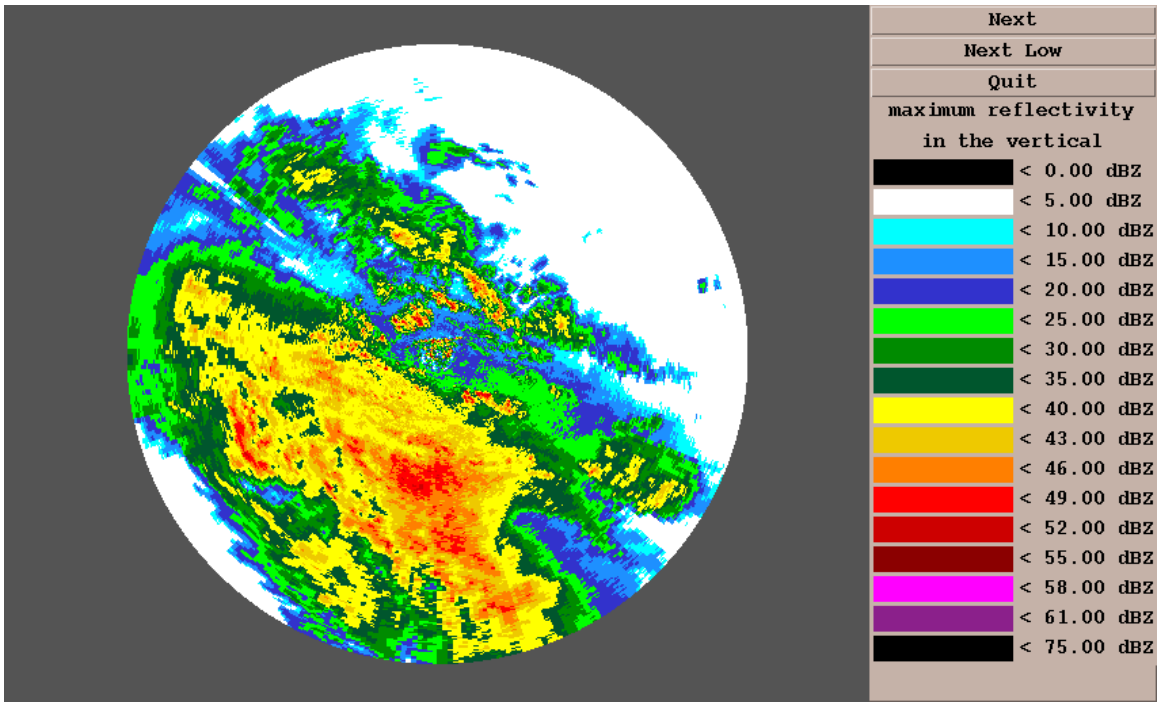

Fig 47 Maximum reflectivity in the vertical, r_x (KOKX_N23993 VS_20)

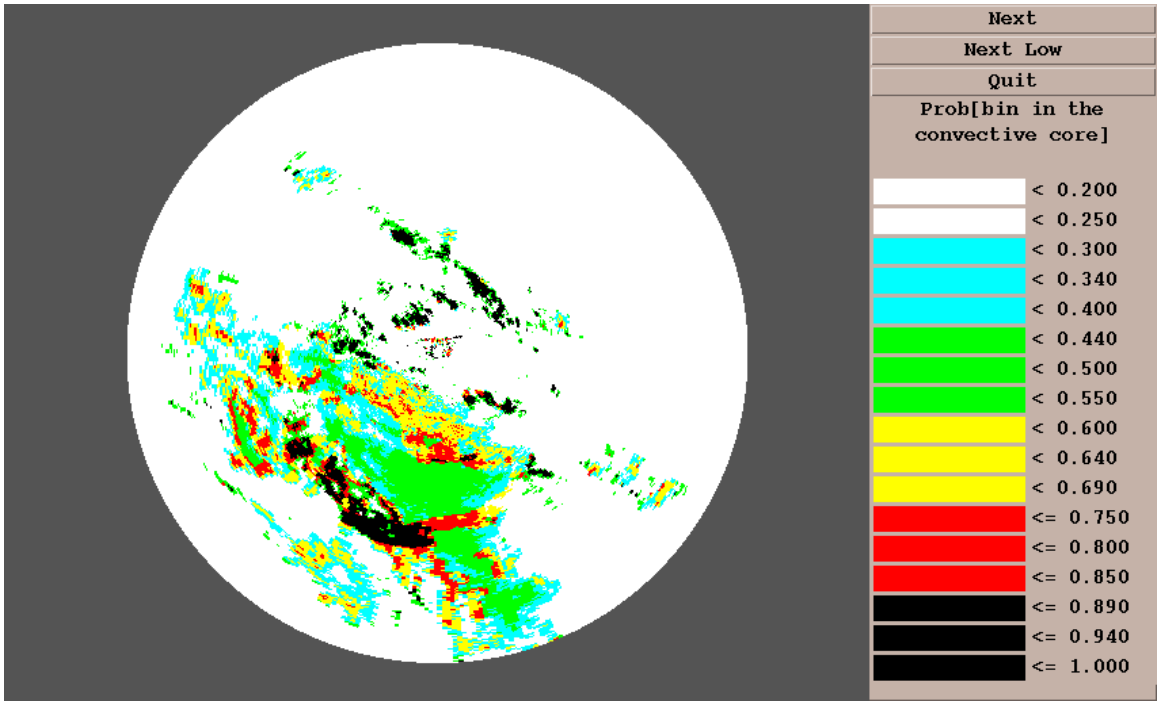

Fig 48 Prob [Bin $\in$ convective | •] (KOKX_N23993 VS_20)

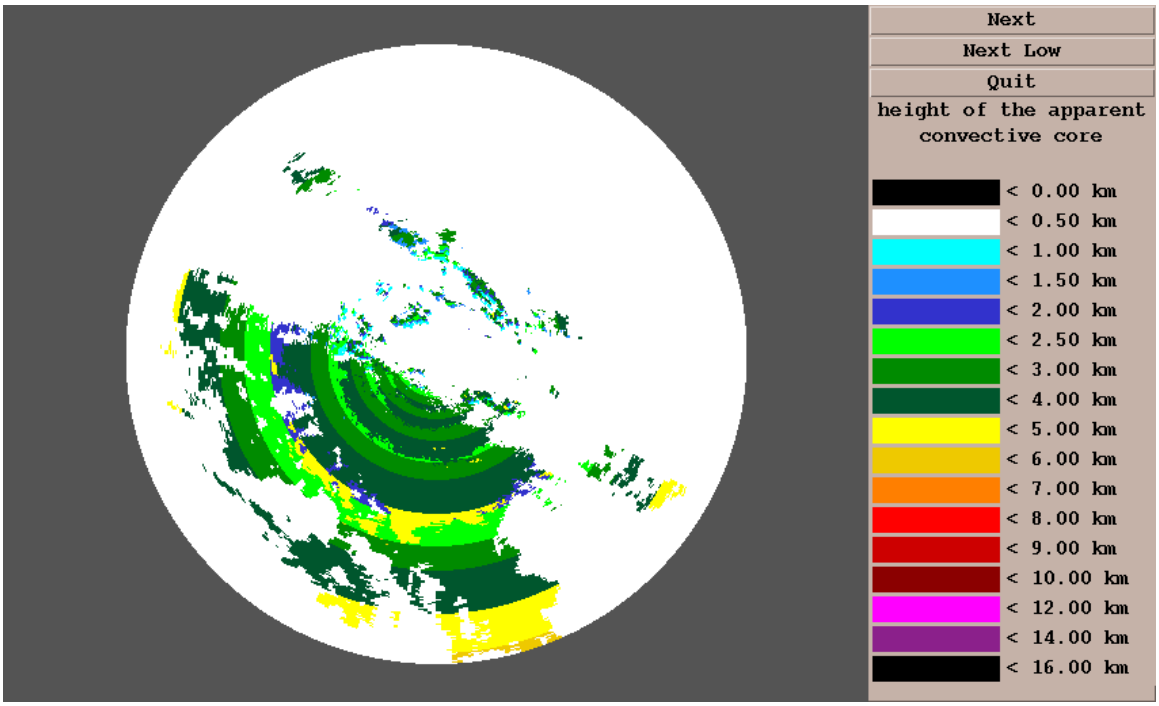

Fig 49 Top height of apparent convective core (KOKX_N23993 VS_20)

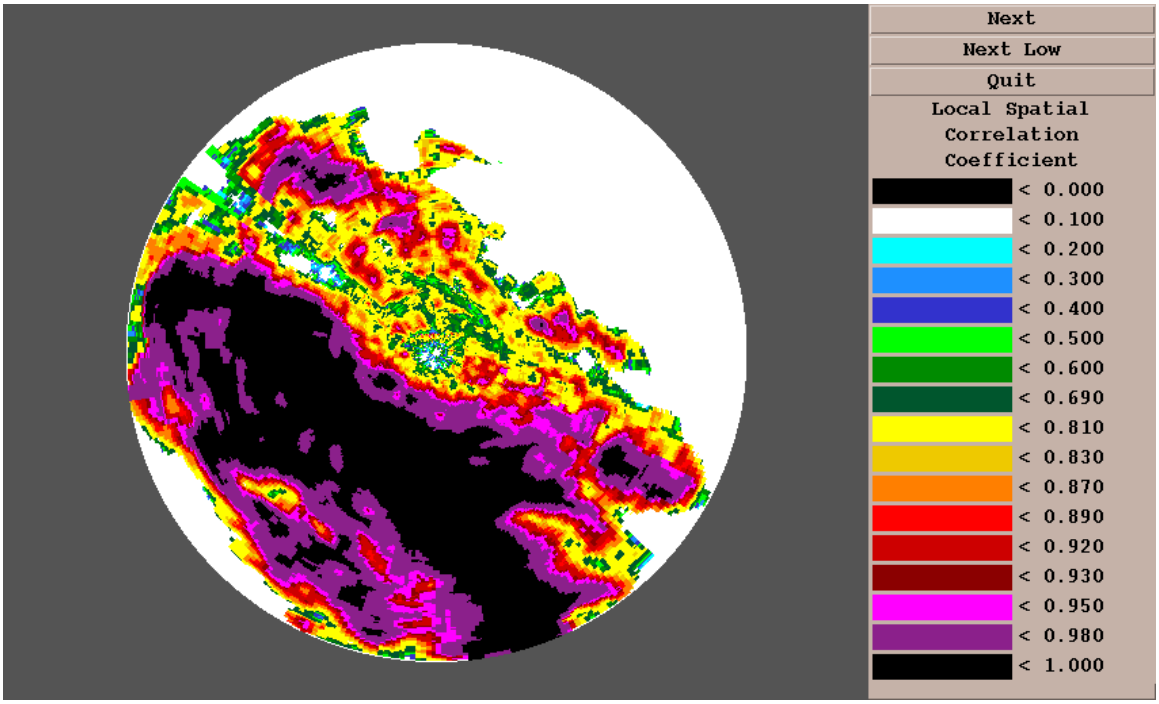

Fig 50 Vertically-averaged spatial correlation of reflectivity, ρ_r (KOKX_N23993 VS_20)

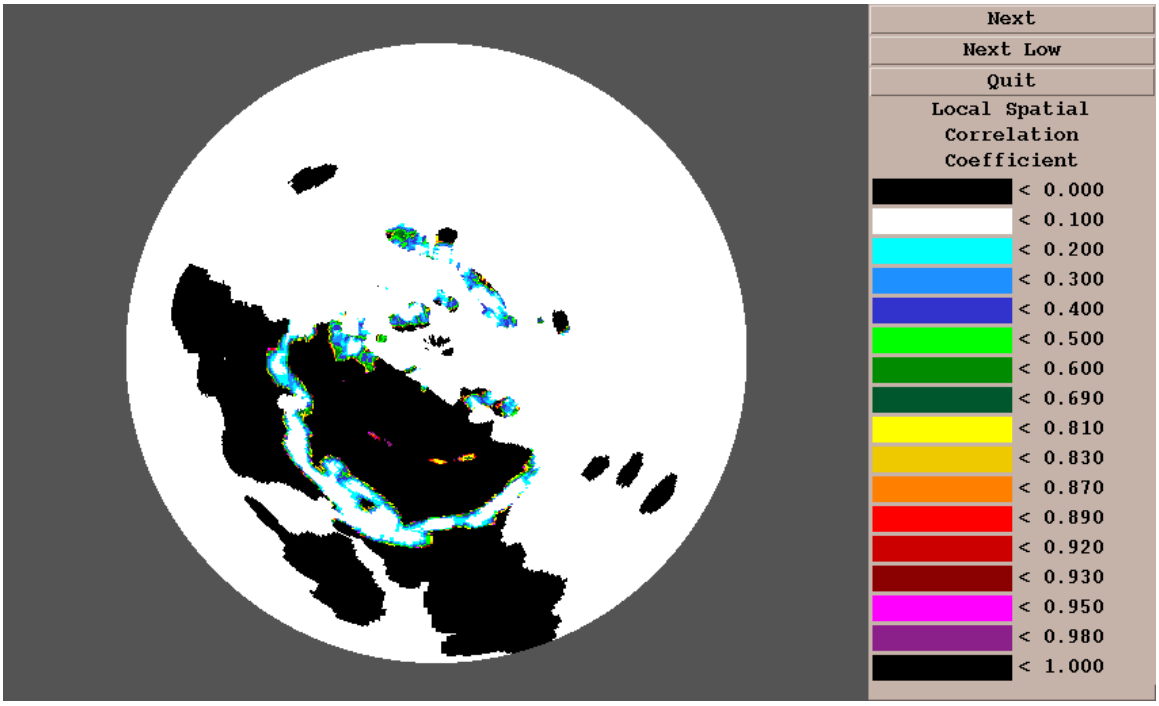

Fig 51 Spatial correlation of height of apparent convective core, ρ_h (KOKX_N23993 VS_20)

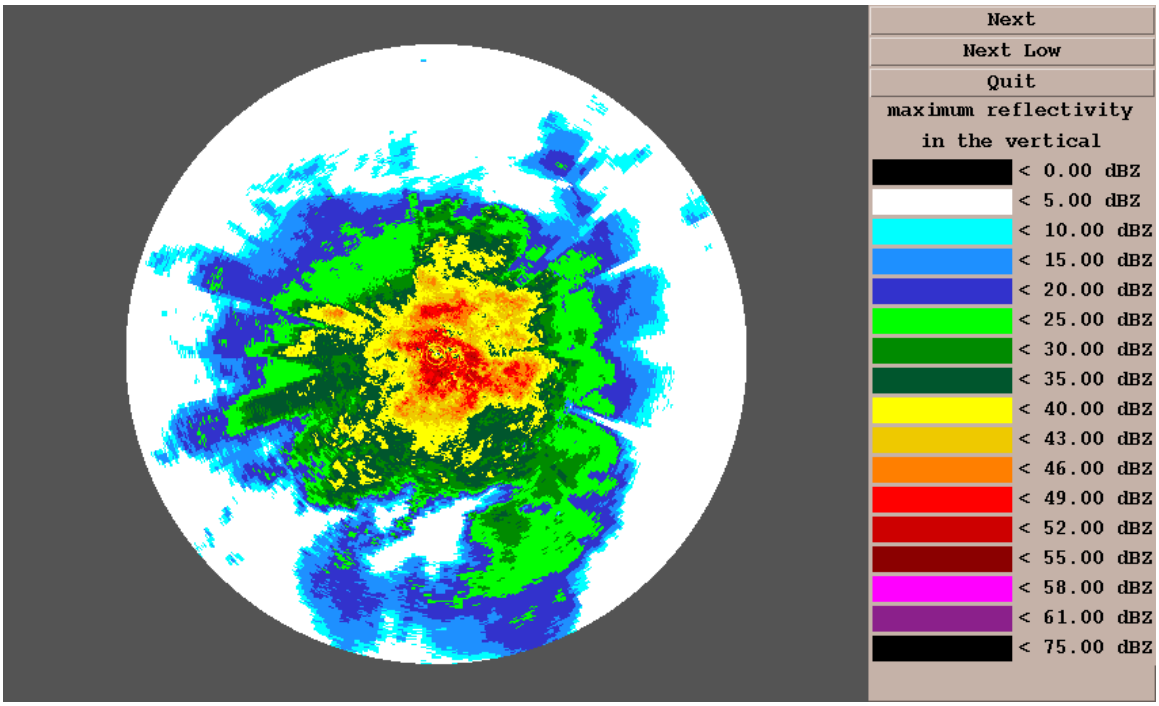

Fig 52 Maximum reflectivity in the vertical, r_x (KRTX_N12384 VS_180)

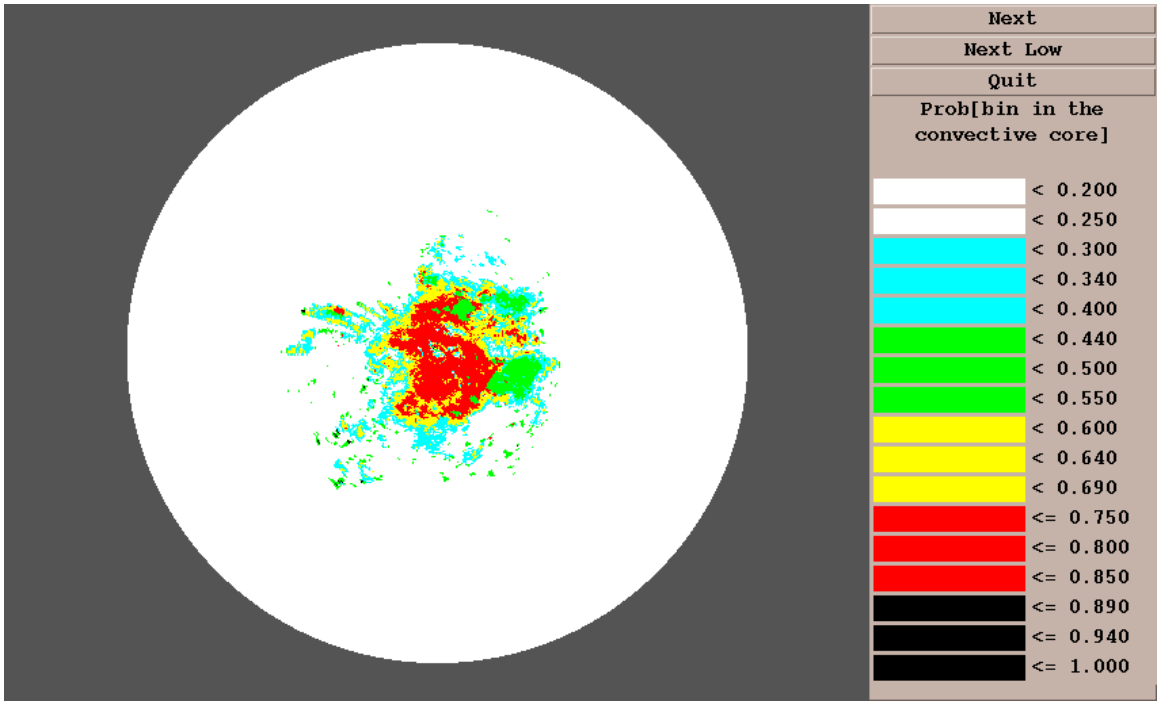

Fig 53 Prob [Bin $\in$ convective | •] (KRTX_N12384 VS_180)

demarcation between the convective and stratiform areas as recognized visually. The 'true' convective core was then assumed to be the area for which r_x exceeds 35 dBZ (an adaptable parameter) in the convective side of the demarcation line. Figs. 2, 4, 6, 9, 15, 17, and 22 show the corresponding Prob[Bin $\in$ convective | •] (= 1 - Prob[Bin $\in$ stratiform | •]) estimated from Eq.(6) for volume scans 245, 255, 265, 275, 285, 295 and 305, respectively.

Throughout this work, the number of thresholds chosen for the attributes was 3 for all; i_{rxc1} = 38 (dBZ), i_{rxc2} = 40 (dBZ), i_{rxc3} = 42 (dBZ), $i_{\rho r1}$ = 0.97, $i_{\rho r2}$ = 0.98, $i_{\rho r3}$ = 0.99, $i_{\rho h1}$ = 0.9, $i_{\rho h2}$ = 0.99, and $i_{\rho h3}$ = 0.999. Visual inspection of the figures indicate that a threshold probability of about 0.87 (i.e. between the color-coding levels of 'red' and 'black' in the probability figures) separates convective cores reasonably well. How the attributes ρ_r and ρ_h may contribute to the discrimination may be seen in Figs. 10, 11 and 12, which show, respectively, the top-height of the apparent convective core, ρ_r and ρ_h. Note that, generally speaking, the larger ρ_r or ρ_h is, the less likely the precipitation is convective.

Although the technique is generally successful in delineating the convective core, a number of deficiencies are readily apparent even in these results from the calibration (i.e. parameter estimation) mode;

1) chunks of areas in the convective core are not identified as convective ('red' non-convective 'islands' in the 'black' convective 'channels'),
2) convective cores at the farthest ranges are not identified as such,

3) there are arcs in the stratiform region misidentified as convective (see, e.g., Fig. 9), and
4) there are blobs in the stratiform region misidentified as convective (se, e.g., Fig. 17).

Issue 1 stems from the fact that mature convective cores have spatially rather uniform reflectivity and top-height of convective core. Initially, use of non-normalized attributes (other than r_x) such as the vertically-integrated liquid water content (VIL, see Fig. 7) and reflectivity gradient in the vertical above the height of maximum reflectivity (see Fig. 13) were purposefully avoided so that the separation technique is rendered as site-independent as possible. The above deficiencies, however, suggest that non-normalized attributes may have to be introduced to the conditioning set in Eq.(6). Issue 2 stems from the fact that both the horizontal and the vertical resolutions are greatly diminished at the farthest ranges. This problem can be addressed by estimating the covariance structure and applying the separation technique in a range-dependent manner. Issue 3 stems from the lack of sampling resolution in the vertical (i.e. VCPs are too sparse). Note in Fig. 9 that the 'black' areas in the stratiform region corresponds to the 'lighter' areas in the same region of Fig. 12. Note in Fig. 10 that these areas correspond to the ranges where sudden 'jumps' (e.g., from 'green' to 'yellow' in the color coding scheme) occur in the top-height of apparent convective core. Such 'jumps' are essentially a VPR effect, and hence are difficult to address with an estimation technique that works in a bin-by-bin manner. In addition to bin-by-bin classification, areal masking may also be necessary to effectively deal with this problem (see, e.g., Fig. 18 in Section 4 of Fulton et al. 2001). The source of Issue 4 is not very clear. Note that the 'black' blobs in the stratiform region of Fig. 17 arises from the 'holes' in the same region of Figs. 19 and 20. These 'holes' occurs because of the small areas of anomalous high top-height of apparent convective core (the 'red' specks) in the stratiform region of Fig. 18, the source(s) of which is unknown at this point.

2.4 Evaluation

For independent evaluation of the classification technique, separation was performed for the following cases and the results are visually examined. To test the robustness of the technique, a wide range of events from various sites were included. Because the separation technique is to support VPR correction, we are not necessarily interested here in quantifying how successful the classification is (which may or may not result in significant improvement in VPR correction). As such, the focus here is on qualitative evaluation of the classification results through careful visual examination. Due to space limitations, it is not possible to include all results. Here, we limit presentation of the results only to a single volume scan per site: they are chosen such that the performance of the separation technique is representative of many other volume scans for the site. Below, we summarized the results for each case. It is reminded here that the covariance structure used in the validation runs is based solely on the single KINX event, and no additional tuning of any kind was performed for the validation.

Table 1. List of cases.

Call Letter	Site	Tape #	Period	Storm Type	Used For
KAMA	Amarillo, TX	N04248	5/30/95	squall line	validation

KATX	Seattle, WA	N10814	2/2/96	stratiform	validation
KDDC	Dodge City, KS	N01158	7/14/93	organized-convective	validation
KEVX	Eglin AFB, FL	N09652	10/4/95	hurricane (Opal)	validation
KFDR	Frederick, OK	N01114	5/9/93	squall line	validation
KFWS	Forth Worth, TX	N02983	4/18/95	squall line	validation
KHGX	Houston, TX	N02961	10/17/94	organized-convective	validation
KICT	Witchita, KS	N02075	4/28/94	squall line	validation
KINX	Tulsa, OK	N04206	5/8/95	squall line	estimation
KMLB	Melbourne, FL	A20054	3/25/92	chaotic-convective	validation
KOKX	New York, NY	N23993	10/19/96	stratiform	validation
KRTX	Portland, OR	N12384	2/6/96	stratiform	validation

KAMA - Misidentification of convective areas in the convective front is evident (the 'red islands' in the 'black channel' in Fig. 24). The misidentification stems from very smooth top-height of apparent convective core (see Figs. 26 and 27). Inclusion of VIL may improve the situation.

KATX - This is a pure stratiform event, and the separation technique correctly identifies the entire area as such.

KDDC - Although the leading edge (below the straight line) is discernable, only the area within the arc of relatively uniform r_x (see Fig. 30) is stratiform. Except for a few 'red islands' in the areas of mature convection and at far ranges (see Fig. 31), the separation is quite successful.

KEVX - Misidentification in the areas of mature convection is glaring. Note in Fig. 34 that the top-height of convective core is spatially very uniform, resulting in large ρ_h (see Fig. 36). As in KAMA, use of VIL as an additional attribute may improve the situation.

KFDR, KFWS - Except for a few 'red islands' and misidentification at the farthest ranges, the separation is very successful.

KHGX - The separation is quite successful except for the far-range convective core in the 11 o'clock direction.

KICT - The separation is very successful except for a few spots in the convective cores.

KMLB - Other than a few 'red islands' in the areas of mature convection, the separation is very successful.

KOKX - A large area in the stratiform region is mis-classified. The misidentification stems from the lack of vertical sampling resolution: note in Figs. 49 and 51 that the abrupt changes

in the top-height of apparent convective core is responsible for smaller ρ_h (and hence the areas of misidentification in the stratiform region). Denser VCPs should improve the situation. Areal masking, based on identification of areas of brightband enhancement, may also be considered.

KRTX - This is a pure stratiform event, and the separation is very successful.

2.5 Summary, Conclusions and Future Research Recommendations

Based on the exploratory analysis summarized in Fulton et al. (2001), a prototype technique for automatic identification and delineation of convective core has been developed and evaluated through visual examination. Using the three attributes identified as the most skillful in FY01; the maximum reflectivity in the vertical, r_x (dBZ), the vertically-averaged local spatial correlation of reflectivity, ρ_r, and the local spatial correlation of the top-height (km) of apparent convective core (reflectivity exceeding 35 dBZ), ρ_h, the technique thresholds the attributes into binary (indicator) variables, and performs optimal linear estimation on the indicator variables. The result is a 230x360 polar map of probability of an azimuth-range (az-ran) bin belonging to the convective core.

To evaluate the performance and robustness of the technique, the indicator covariance structure was estimated from a single squall line event in Tulsa, OK. Then, the technique was applied to 11 other cases from 11 different sites using the same indicator covariance. Visual examination of the results from both the parameter estimation and the independent validation phases of the work indicates that:
1) the technique performs reasonably well for a wide range of events and sites, but
2) it tends to misidentify pockets of mature convection and at the farthest ranges of the radar.

The results also suggest that the technique may be improved by introducing additional attributes in the conditioning set such as the vertically-integrated liquid water content (VIL), even if the use of such a site- and seasonality-dependent attribute may compromise robustness of the technique. Other deficiencies of the technique are traced to the lack of sampling density in the vertical (i.e., sparse VCP), and hence are more difficult to address. The analysis carried out in this work should be repeated using data from new (denser) VCPs before areal masking is considered for the technique.

Because convective-stratiform separation is to support VPR correction, its performance must ultimately be gauged through evaluation of the coupled application of convective-stratiform separation and VPR correction. It is recommended that:
1) inclusion of additional attributes be investigated to mitigate misidentification in the areas of mature convection, and
2) performance of the separation technique be quantitatively evaluated through application of VPR correction.

Computationally, the probability-estimation part of the separation technique described in this work is trivial: it requires solving a small linear system only once. On the other hand, calculation

of the locally-averaged attributes in the prototype code, as is, is computationally rather intensive. An efficient scheme for calculation of local statistics, such as successive addition and subtraction employed in the Multi-sensor Precipitation Estimator (MPE), must be implemented to improve the operational viability of the technique.

References

Deutsch, C. V. and A. G. Journel, 1992: GSLIB Geostatistical software library and user's guide. Oxford University Press, 340pp.

Fulton, R., D. Miller, J. Breidenbach and D.-J. Seo, 2001: Final Report Interagency MOU among the NEXRAD Program, The WSR-88D Radar Operations Center, and The NWS Office of Hydrologic Development. Hydrology Laboratory, Office of Hydrologic Development, National Weather Service, Silver Spring, MD.

Schweppe, F. C., 1973: Uncertain dynamic systems. Prentice-Hall, 563pp.

Seo, D.-J., 1996: Nonlinear estimation of spatial distribution of rainfall - An indicator cokriging approach. Stoch Hydrol Hydraul, 10, 127-150.

Seo, D.-J., J. Breidenbach, R. Fulton, D. Miller and T. O'Bannon, 2000: Real-time adjustment of range-dependent biases in WSR-88D rainfall estimates due to nonuniform vertical profile of reflectivity. J Hydrometeor, 1, 222-240.

Vignal, B., G. Galli, J. Joss and U. Germann, 2000: Three methods to determine profiles of reflectivity from volumetric radar data to correct precipitation estimates. J Appl Meteor, 39(10), 1715-1726.